ANNALS OF GEOPHYSICS, 68, 5, DM576, 2025; doi:10.4401/ag-9350
OPEN ACCESS

A proposed workflow to characterise site conditions and reference potential for Greek AdriaArray stations

Antonia Papageorgiou[*,1,2], Olga-Joan Ktenidou[1], Kalliopi-Elli Fragouli[1], Vasilis-Erion Pikoulis[2], Spyros Liakopoulos[1], Fanis Halaris[1]

(1) Institute of Geodynamics, National Observatory of Athens, Lofos Nymfon-Thiseion, Athens, Greece
(2) University of Patras, Patras, Greece

Article history: received April 7, 2025; accepted November 5, 2025

Abstract

In Greece, the 1Y AdriaArray network consists of 31 stations, covering most of the mainland. Although all of them are considered to lie on rock formations, the validity of the reference station assumption has not been verified yet – and neither has it been investigated throughout the rest of the extensive AdriaArray network. In this study, we attempt a systematic compilation of station metadata and site conditions for Greek 1Y stations, coupled with an in-depth empirical analysis of weak- and strong-motion recordings to estimate site effects. We wish to propose this as a basis for a structured workflow for documenting station and site conditions information across AdriaArray in a consistent and comprehensive way that can be harmonized across all agencies and countries. We have integrated waveform-derived parameters, focusing on site response and near-surface properties and parameters based on the analysis of external sources, such as geological maps, topographic maps, etc. Single-station amplification functions (horizontal-to-vertical spectral ratios, HVSR) were estimated from the seismic data, and the site resonance characteristics were assessed, not only in the conventional way of combining components, but also assessing directional sensitivity. Based on the various criteria investigated, we characterize stations with respect to their potential capacity as reference.

Keywords: Station characterisation; Reference sites; Geological conditions; Topographic slope; Site amplification

1. Introduction and motivation

AdriaArray is a collaborative multi-national effort aimed at monitoring the Adriatic Plate and its active margins in the central Mediterranean in a comprehensive way through a dense network of broadband seismic stations. This extensive seismic array intends to enhance our understanding of active tectonics and volcanic activity in the region. The AdriaArray region reaches from the Massif Central in the west to the Carpathians in the east, from the Alps in the north to the Calabrian Arc and mainland Greece in the south.

With 64 participating agencies from 30 countries, 1068 permanent and 440 temporary broadband stations from 23 mobile pools (Fig. 1), AdriaArray (Kolínský et al., 2024, 2025) presents challenges as well as opportunities

in terms of coordinating and harmonising both data analysis by the various scientific disciplines across regions, as well as metadata compilation and the characterisation of roughly 1500 stations. This paper focuses on the metadata related to the stations, not from the point of view of hardware (e.g. sensor corner frequencies, as discussed in Kolínský et al., 2025) but from the point of view of site characterisation in the broader sense, as typically considered by the strong-motion and ground-motion communities.

The pioneering global ground-motion databases NGA-West2 (Ancheta et al., 2014) and NGA-East (Goulet et al., 2021) that laid some of the foundation for strong-motion data processing prioritised the collection of rich and homogeneous metadata to accompany their data. They introduced the notion of the 'flatfile' as a means of compiling such metadata in a tabulated format, along with data-derived values such as peak and response spectral values. Flatfiles include information related to the source, the station, or the specific source-station combination (i.e. the recording). NGA flatfiles were very rich in station metadata in terms of geological and geotechnical descriptions, near-surface Vs estimates including qualifiers, depth to bedrock estimates according to several definitions, etc. European databases soon followed along the path paved by the NGA groups, e.g. ESM (Luzi et al., 2016; 2020; Lanzano et al., 2021; https://esm-db.eu/) within the framework of ORFEUS.

Ground motion models, as they advance, have incorporated more detailed descriptors of station conditions, leading to a global increase in the effort for characterising stations. One of the most important reasons for characterising stations is the potential for site amplification introducing bias to downstream uses of data. Although in the past it was thought that site amplification is an issue mostly for accelerometric data, often recorded at stations installed on sediments, it is now clear that rock stations do not always exhibit the ideal response often assumed. Several studies in the past decade or so turned their attention to rock sites.

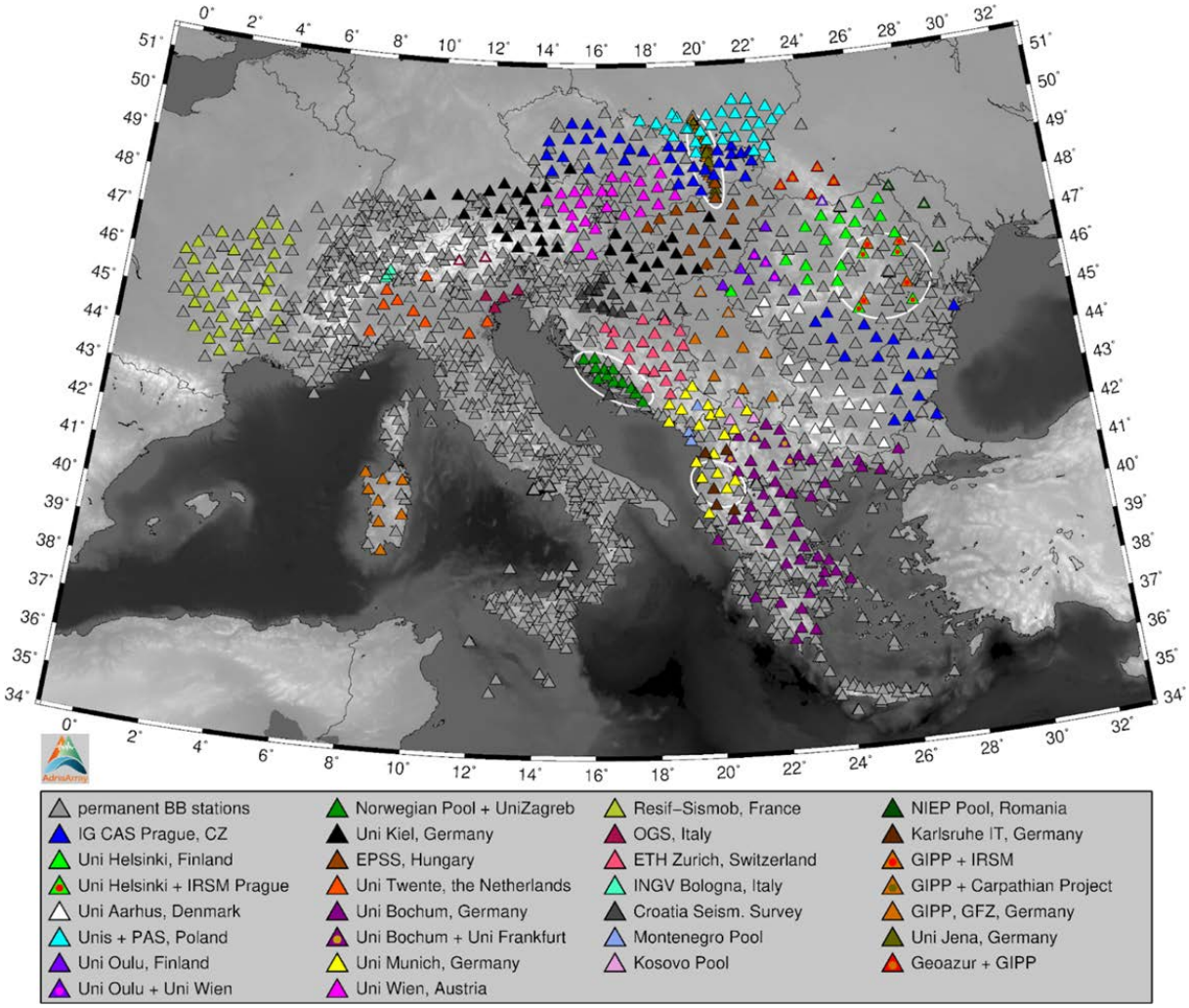

Figure 1. Map of all permanent broadband, short-period and strong motion stations (from Kolinsky et al., 2025).

Van Houtte et al. (2012) examined stations in Christchurch that were typically used as reference stations without prior validation and assessed their reference capacity based on the estimation of empirical site transfer functions. Ktenidou and Abrahamson (2016) identified broadband amplifications at rock sites in Central-Eastern North America, considered as extremely hard rock (Vs30 of 2000 m/s). European initiatives such as Lanzano et al. (2020) and Pilz et al. (2020) attempted to assess reference stations in Italy and Europe respectively. Di Giulio et al. (2021) reviewed European station characterisation efforts and stressed the importance of consistency. Panzera et al. (2024), on the other hand, considered worldwide databases to identify appropriate ground motions as reference, taking the process further into spectral matching. The effort described here follows upon a recent effort that took place in Greece.

Ktenidou et al. (2024) studied the HL network, operated by the National Observatory of Athens (NOA), which includes both strong-motion and broadband stations. They focused on HL stations installed on – or thought to be installed on – rock, aiming to investigate how reliable they were, both in terms of station metadata and in terms of seismic response. To this aim, on the one hand they compiled several descriptors from as many external sources as possible, including official operator or database websites, literature, as well as studying geological maps ad hoc, and combined this with observations from the network operator's site visits. On the other hand, they compiled and curated a hand-picked strong-motion database for the stations under study and derived station amplification characteristics from empirical spectral ratios. They ultimately co-assessed all types of station information to evaluate the overall potential of their stations as reference sites. It is noted that ESM includes several station metrics and metadata but those are limited to accelerometric stations, while the effort of Ktenidou et al. (2024) also extended to seismological broadband stations implicitly assumed as reference sites.

Following upon this precedent, the goal of this work is to apply such a workflow to the Greek AdriaArray stations of the 1Y network and ultimately propose a systematic workflow for documenting station information and particularly site conditions across all of AdriaArray, in a consistent and comprehensive way that could potentially be harmonized across the various agencies and countries participating in this international effort.

This idea has already been proposed and discussed within the AdriaArray consortium, in the Engineering Seismology Collaborative Research Group (CRG), and the article at hand is the proof of concept. We envision eventually having three types of descriptive site parameters in terms of the sources of the station information: (1) waveform-derived parameters, focusing on site response and near-surface properties (e.g. site transfer function from recorded ground motion, fundamental frequency, etc.); (2) parameters based on the analysis of external sources, such as geological maps, topographic maps, DEMs, etc. (e.g. surface geology, slope and near-site topographic features; potential for noise; housing); and (3) operator's observations (including photographs) on any of the previous parameters, in addition to detailed information in the installation conditions. This kind of 'inside information' from the operators can be especially critical given the array's partially temporary nature, and we consider it perishable data for all stations planned to be removed in the future.

Of the above types of sources, the first two (waveform and external source analysis) can be achieved through simple desk studies, while the third one (operator's feedback) may require a site visit and walkover if the documentation from past visits is not adequate. The upside is that for the temporary stations, there will always be at least one more chance for a walkover within project budget, when the time comes to remove the stations. Hence we believe that the proposition we make will not incur any significant cost to the various operating agencies.

In this article, we present the results of the desk study conducted for Greek AdriaArray stations, including the first two steps mentioned above (waveforms and external sources). In the next phase envisioned for this work, we will join forces with the four operating agencies in Greece to solicit information from site walkovers.

2. Study area

To kickstart this endeavour, the idea is applied to Greece, where the 31 Greek stations of the 1Y network cover most of the mainland, as seen in Fig. 2 (we do not consider the 4 stations from Northern Macedonia that share the 1Y code). As indicated by the 'H?' codes noted on the map, these stations are maintained by the four network operators in Greece, namely the National Observatory of Athens (HL), the University of Thessaloniki (HT), the University of Patras (HP), and the University of Athens (HA). The station codes begin with GR, followed by 2 numerical characters. Table 1 gives some basic metadata for the stations.

We note that in the two cases where a station was moved, on the islands of Corfu and Evia (GR19 and GR27), the location with the largest number of recordings so far is indicated with a triangle, while the one with the fewest

Table 1. Some basic metadata of the Greek 1Y AdriaArray stations.

Station code	Channel	Station name	StLat (deg)	StLon (deg)	StEl (m)	Start date
GR01	HH	Neo Petritsi, Serres	41.28523	23.29062	219	2022-09-29T06:30:00
GR02	HH	Drama	41.15982	24.15955	238	2022-09-29T10:40:00
GR03	HH	Xanthi	41.14978	24.88246	296	2022-09-28T10:00:00
GR04	HH	Abdera	40.98043	24.96409	143	2022-09-28T12:12:03
GR05	HH	Maronia-Sapes, Petrota	40.86866	25.59893	69	2022-09-29T06:30:00
GR06	HH	Mavrokklisi	41.33885	26.27182	277	2022-09-30T10:26:38
GR07	HH	Mesimeri, Edessa	40.78446	22.02076	506	2022-09-28T16:30:00
GR09	HH	Rentina	40.66019	23.68722	80	2022-09-29T15:27:29
GR10	HH	Kriovrisi, Ptolemaida	40.48323	21.59428	781	2022-09-28T12:00:00
GR11	HH	Veroia	40.52277	22.18965	300	2022-10-13T08:00:00
GR12	HH	Katachas	40.47087	22.54196	130	2022-10-04T14:00:00
GR13	HH	Katsika, Petralona	40.35163	23.18590	300	2022-09-29T11:32:26
GR14	HH	Doliana	39.90004	20.57880	570	2022-10-01T14:18:25
GR15	HH	Vouvousa	39.94093	21.04702	1016	2022-10-01T09:17:50
GR16	HH	Livadero	40.04160	21.93832	1101	2022-09-28T10:23:00
GR17	HH	Meteora, Kalambaka	39.73374	21.63067	493	2022-10-04T11:40:37
GR18	HH	Lakeria	39.72811	22.66836	1031	2022-09-28T16:43:28
GR19B	HH	Vitalades, Lefkimmi	39.40469	20.01632	114	2023-06-14T16:30:00
GR20	HH	Itamos	39.23506	21.74635	836	2022-09-29T12:26:35
GR21	HH	Thetidio	39.37262	22.51318	366	2022-10-04T13:41:13
GR22	HH	Monastery Panagia Xenia, Sourpi	39.08948	22.82636	333	2022-10-07T11:55:27
GR23	HH	Rovies	38.80762	23.22900	67	2022-09-30T14:18:27
GR24	HH	Mousounitsa	38.68870	22.19439	893	2022-09-28T12:30:00
GR26	HH	Sagmata Monastery, Theva	38.39999	23.41070	782	2022-09-22T12:00:00
GR27	HH	Kouvelles, Euboea	38.18244	24.23306	105	2022-09-28T15:11:00
GR28	HH	Kastro	37.88988	21.14024	236	2022-12-22T09:00:00
GR29	HH	Doxa	37.70421	21.92254	630	2022-10-05T16:35:52
GR30	HH	Achladokambos	37.52174	22.57738	483	2022-10-04T09:03:51
GR31	HH	Kephalas	37.03306	22.52121	379	2022-10-05T07:32:00
GR32	HH	Zarakas	36.96712	22.98759	75	2022-10-04T13:58:45
GR33	HH	Lefktro	36.76218	22.33366	424	2022-10-05T11:23:51

is indicated by a grey circle. In this work, we will not show results from the latter stations, namely station GR27B, moved only recently (March 2025) from Kouveles to Elaiochori (Evia), nor from GR19, moved some months after its initial installation from Vitalades to Marathias (Corfu), where it remains and has recorded the largest number of earthquakes.

Figure 2. Map showing the location of the 31 AdriaArray stations in Greece. Town/city names and operator codes (Hx) are included along with the station code (GRxx).

3. Waveform-derived parameters

3.1 Database compilation

The dataset analyzed in this study consists of over 4,000 waveforms recorded by the 32 Greek 1Y broadband stations within a 2-year period: from September 2022 – which is roughly when the AdriaArray stations began to operate in Greece – and up to September 2024. We used the catalogue provided by NOA (https://eida.gein.noa.gr/fdsnws/availability/1) to search for recordings based on criteria of magnitude and distance. Initially, we selected events with ML ≥ 3.5, but because this led to very heterogeneous populations across stations, where needed we progressively included events down to ML ≥ 2.0, taking into consideration the regional seismic activity levels and the source-to-station distances, in order to ensure adequate signal quality across the network. Figure 3 shows the overall distribution of local magnitude and epicentral distance for all data analysed in this study across all stations, along with a histogram of data population per station. All individual station-specific plots can be found in Fig. A1 (parts a,b,c) of the Appendix.

We retrieved raw waveform data and station metadata (XML files) from EIDA@NOA and applied instrument correction to retrieve physical units. We then used our in-house software, inspired by the PEER-NGA methodology described in Kishida et al., 2016 and Goulet et al., 2014, for visual inspection, quality assessment, and waveform processing in both the time and frequency domains. The processing included windowing, signal-to-noise ratio (SNR) evaluation, and filter corner picking.

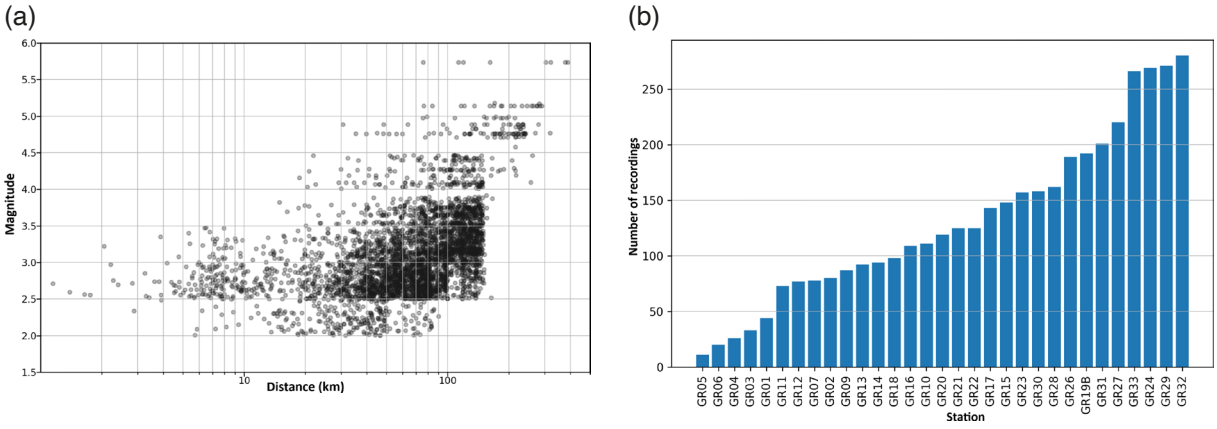

Figure 3. (a) Distribution of magnitude (ML) and distance (epicentral) for all data analysed in this study. (b) Number of recordings used per station.

The first step in the data analysis workflow is to check raw data for clipped waveforms and reject them. This is followed by visual inspection of the velocity traces in the time domain. The software applies an automatic windowing based on the origin time: it identifies P- and S-wave arrivals, computes a realistic S-wave window based on magnitude (not so significant for the small events we have here) and distance, and ensures an equal duration for the pre-event noise and signal windows (Fig. 4, top line). In the signal window, all wave packages after S-wave arrival which are relevant to engineering applications are included. All automatic phase picks (dotted lines) are reviewed and manually adjusted (solid lines). Next, we perform visual inspection in the frequency domain, assessing signal and noise Fourier amplitude spectra (FAS) of acceleration (Fig. 4, lines 2-4). Aside from the signal-to-noise ratio (SNR = 3 threshold), we also considered the fit of the omega-square source model (Brune 1970; 1971 – see dashed red line). In the example of Fig. 4, the vertical red and green lines are the lowest and highest usable frequencies (LUF, HUF) chosen after inspection in both logarithmic and linear frequency scale. Identifying LUF and HUF is important because in what follows, all FAS will only be utilised within their usable frequency ranges to compute the empirical transfer functions. Thus, the results at the high and low frequency ends of the band will not suffer from artefacts.

3.2 Earthquake spectral ratio

The S-wave window onset is taken early enough so as to avoid any effects on the first S waves by the tapering. The end of the signal window is taken not as the end of the direct S waves, but as the end of the strongest part of ground motion, which may also include strong surface waves if applicable. This decisioni s made as per the recommendations of PEER processing practice and is described in more detail in Kishida et al. (2016) and Ktenidou et al. (2021). The acceleration Fourier Amplitude Spectra (FAS) was computed and smoothed using a Konno and Ohmachi (1998) b = 40 mild smoothing. Horizontal-to-vertical spectral ratios were computed as a first approximation of site amplification (HVSR; Lermo and Chavez-Garcia, 1993) for each horizontal component of each recording at each station. The mean HVSR per site was computed as the log average across all events, as is customary, and as Ktenidou et al. (2011) showed that spectral ratio ordinates are lognormally distributed. At each frequency, the mean is computed using only the available recordings within the valid bandwidth, i.e. within the LUF and HUF determined in the previous step. The two components of each FAS are then combined as the square root of the sum of squares (SRSS) to obtain an orientation-independent estimate. With this analysis, we evaluate if the selected

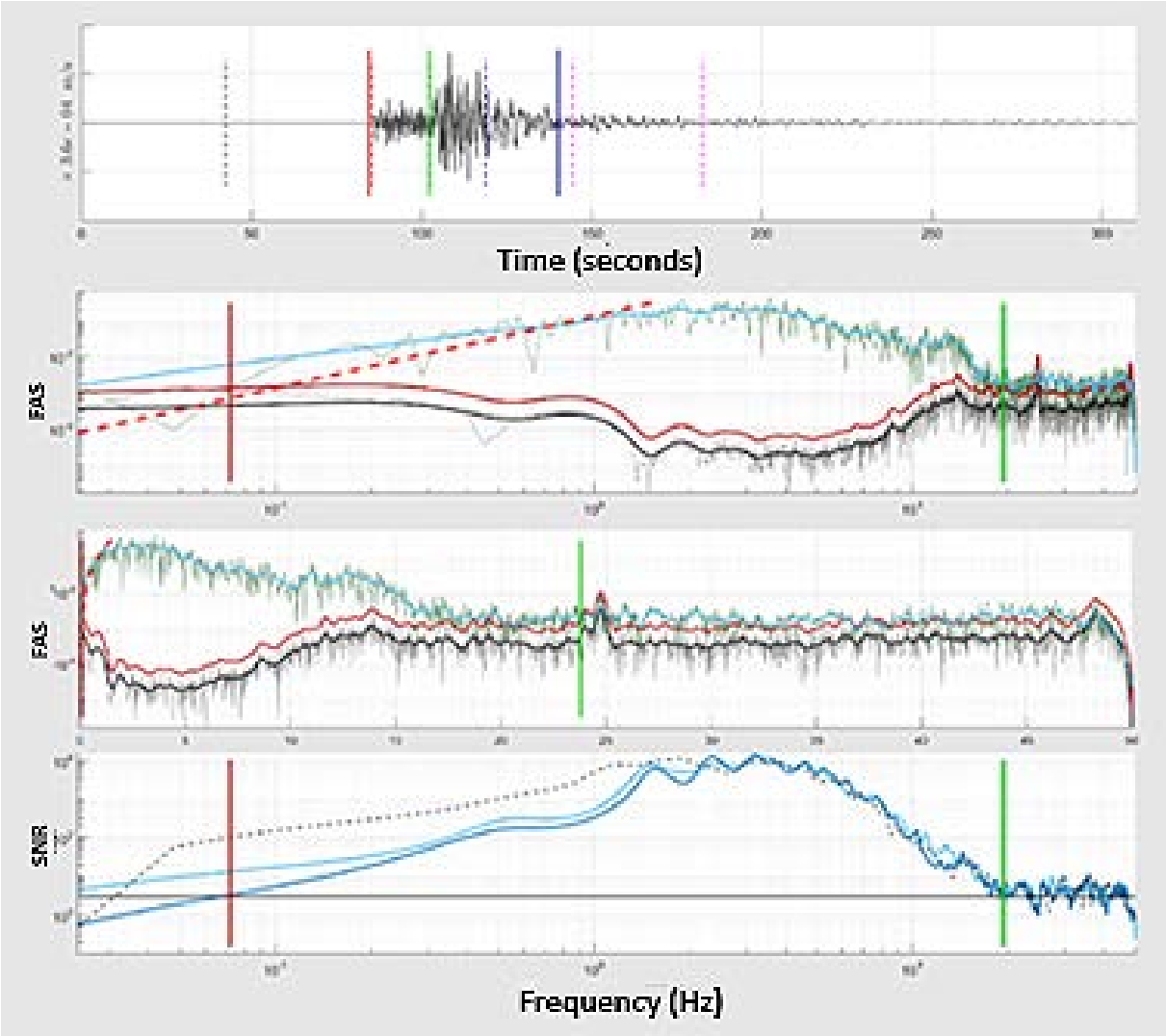

Figure 4. Example panels of manual processing. Top to bottom: windowing of a velocity trace in the time domain, selecting the HUF and LUF in the frequency domain (in logarithmic and linear scale respectively) for the two horizontal acceleration FAS, and inspection of the SNR.

sites behave as expected – i.e. as reference stations- and we single out unexpected responses to investigate further. As stations are assumed to lie on rock, we expect a flat HVSR close to unity. Given HVSR method uncertainties, we only consider as significant amplitude values above 2.7.

While many stations exhibited relatively flat HVSRs without clear resonant peaks, others showed strong amplitude at various frequencies, which is not what we expect of reference sites. Figure 5 presents some characteristic examples. 1Y.GR10 has a very flat, virtually ideal HVSR well below 2 even out to 30 Hz. 1Y.GR12 on the other hand shows a broadband, near-flat amplitude over 2.5 up to 3 Hz followed by a rapid drop, which however could be linked to a strengthening of the vertical signal. 1Y.GR09 and 1Y.GR15 show strong amplitude up to 5 or 6 at 4-5 Hz and 8-9 Hz respectively, which are not in agreement with the flat HVSR of rock sites and are rather more representative of stiff soil profiles with a significant impedance contrast (B class as per EC8; CEN, 2004). Our analysis indicates that, out of the 31 1Y stations, 22 exhibits acceptable mean HVSR shapes. Figure A2 (parts a,b,c) in the Appendix shows individual results for all stations. We note that only for site GR14 do we identify a second peak, i.e. a potential higher mode.

Based on the results of the 31 stations, we seek to create groups of similar responses using hierarchical agglomerative clustering on the mean, orientation-independent HVSR. The method starts with each observation in its own cluster (of size 1) and builds a cluster hierarchy by iteratively merging the closest pair each time. The resulting hierarchy is pruned by defining a maximum intercluster distance or by specifying a number of clusters. We used the Euclidean distance as distance metric and the scikit-learn library as our tool.

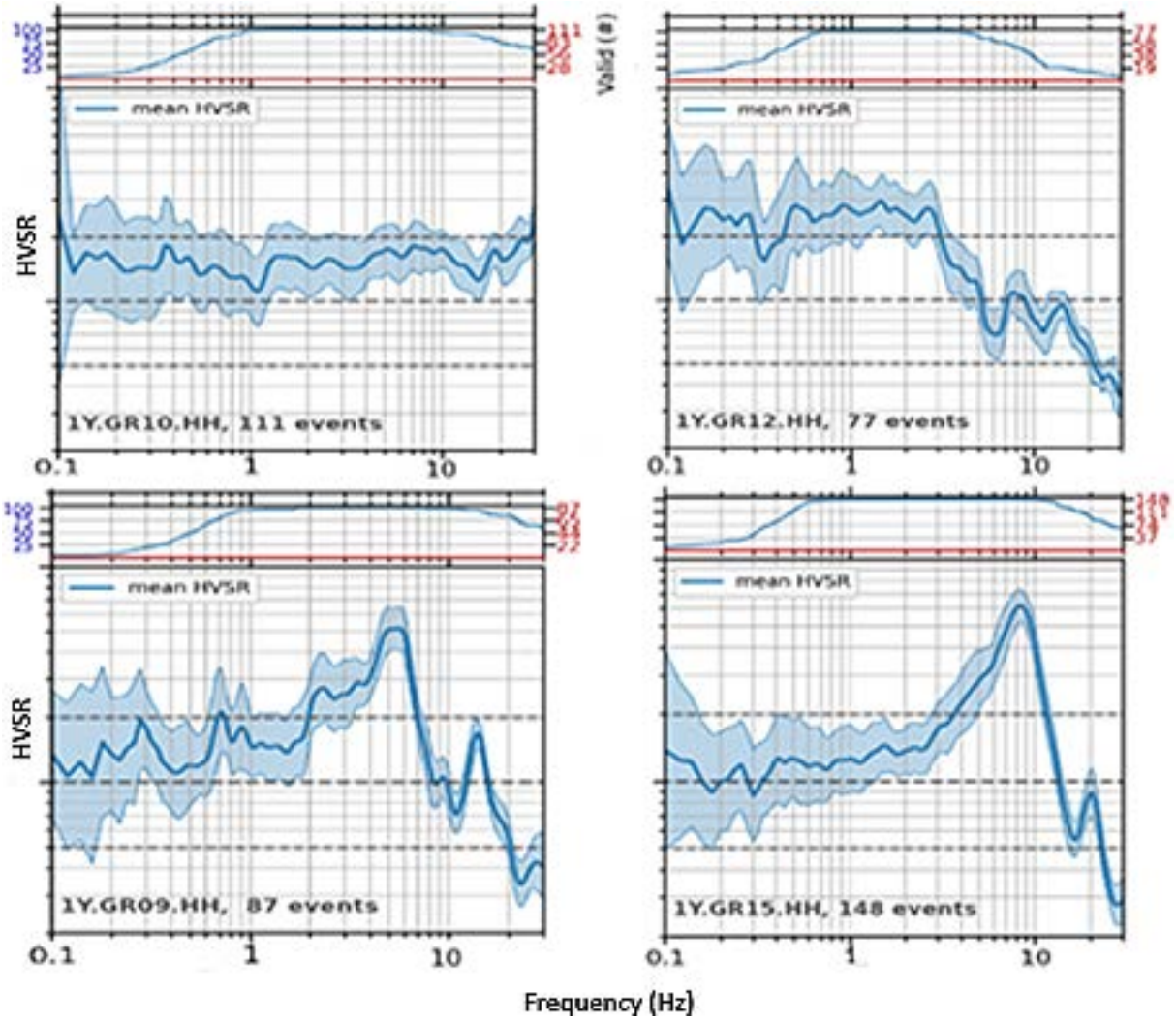

Figure 5. Mean, direction-invariant (SRSS) HVSR ±1 standard deviation results for stations 1Y.GR10, 1Y.GR12, 1Y.GR09 and 1Y.GR15. Inset on top indicates the absolute number (red) and percentage (blue) of usable recordings averaged per frequency.

Figure 6 shows the 4 clusters derived from our analysis of the HVSR curves. Clusters 2 and 4 are near reference. Clusters 1 and 3 show medium- and high-frequency (MF and HF) amplitude and would not be considered as reference sites. Other ways to group are possible by constraining the algorithm parameters, mostly focusing on specific bandwidths.

In addition to not amplifying strongly, a reference site should also have minimal directional sensitivity, i.e. dependency on the orientation of the sensor. Sensors are typically orientated at N000 and N090, which is convenient for networks but completely arbitrary compared to the local geomorphology that may affect ground motion, such as surface topography, basin edges, lateral stratigraphic discontinuities, etc. Such geomorphological site features may cause stronger amplification in given directions, e.g. radial or parallel to the feature. Spudich et al. (1996) first investigated ground motion directionality with spectral ratios when studying topographic amplification, a par excellence directional effect in 2D or 3D. Much later, Ktenidou et al. (2016) proposed a simple way to assess the sensitivity of site response to azimuth, by rotating the as-recorded time series successively by small increments (e.g. 10°) and recomputing the spectral ratios each time, and in Ktenidou et al. (2024) simple statistical metrics were introduced to quantity such sensitivity. By doing so, we can detect and quantify directional variability of HVSR. Strong directionality indicates departure from the assumed 1D behaviour, likely due to local site conditions, and hence departure from the ideal behaviour of a reference site.

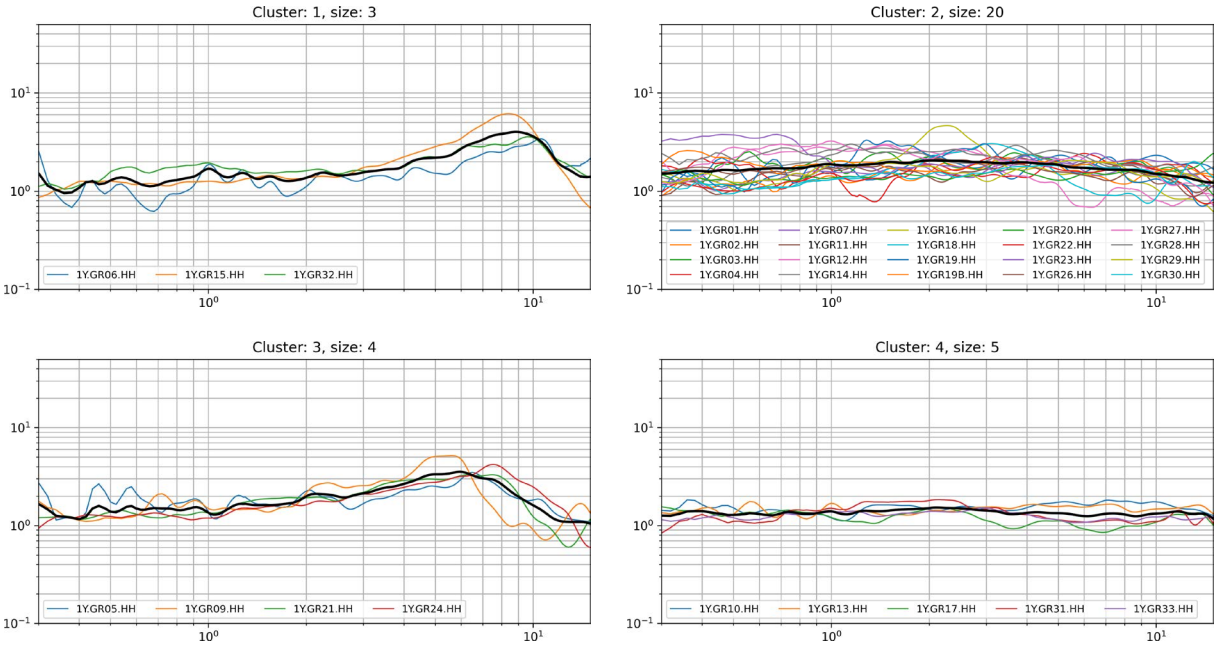

Figure 6. Clusters based on mean HVSR.

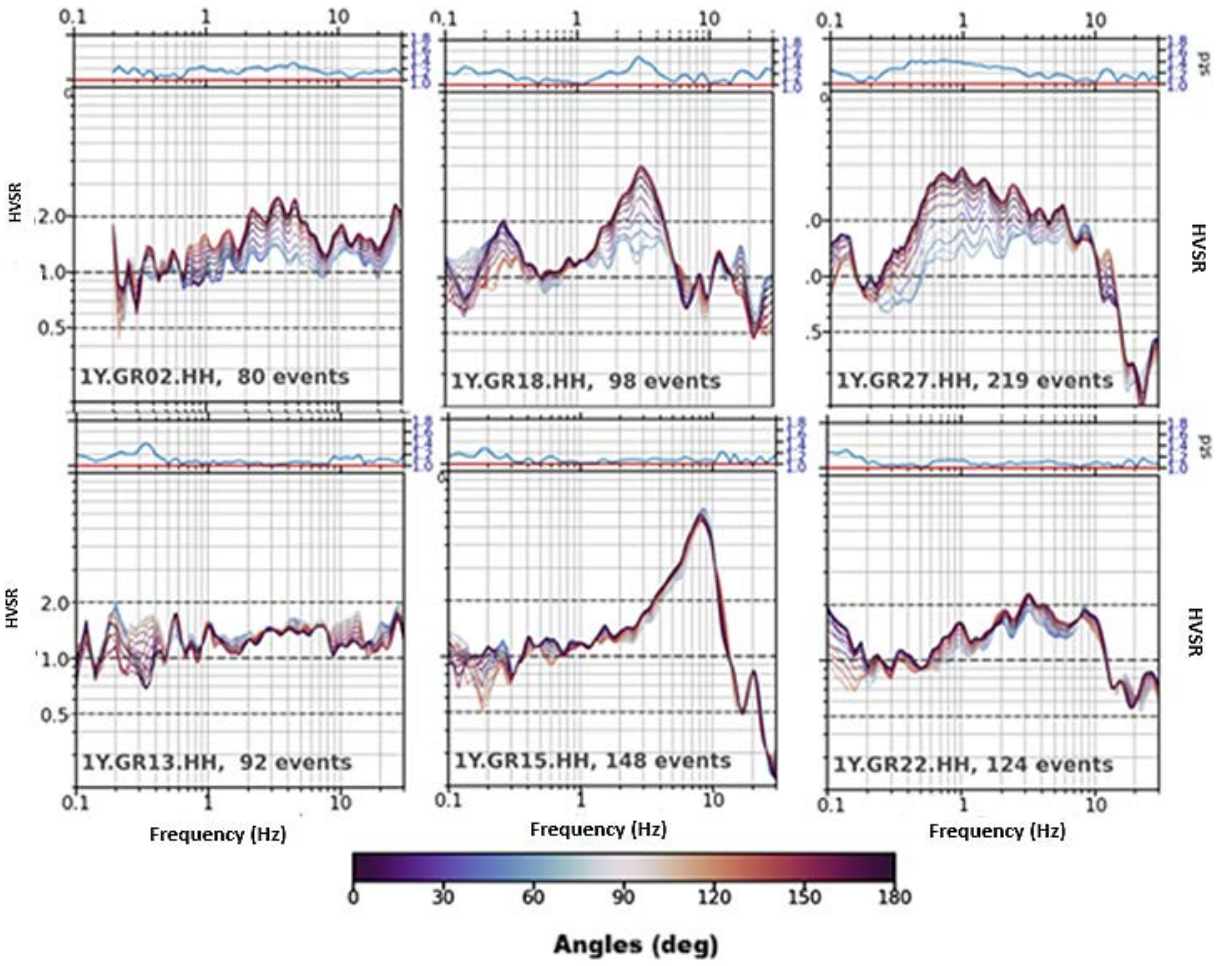

Figure 7. Examples of HVSR rotational sensitivity, from low (lower row) to high (higher row).

Figure 7 illustrates some examples. The bottom row shows very stable responses, regardless of their shape. GR13 has an excellent and GR22 has a good HVSR shape, and they both also exhibit low directionality, making them good reference station candidates. GR15 on the other hand is directionally insensitive but its mean shape is completely inappropriate. The top row shows very sensitive responses, regardless of their shape. GR02 has a good mean shape but is highly sensitive, while GR18 and GR27 have both an inappropriate mean shape and directional sensitivity. Figure A3 (parts a,b,c) in the Supplement shows the HVSR rotational sensitivity for all stations.

Insets on top of each plot show the standard deviation (SD) of HVSR values across all rotations, as an indicator of 1D behaviour (e.g. SD is about 1.06 at GR13 vs. 1.45 at GR18, where peak amplitude A0 varies by more than a factor of 2 with rotations). We use the SD values to estimate stability metrics per station for specific frequencies: at the resonant frequency (SD_f0) and in characteristic ranges, namely 1-10 Hz (of most usual engineering interest) and 0.3-30 Hz (a wider band encompassing all potentially interesting frequencies). Figure A3 (parts a,b,c) in the Appendix shows individual results for all stations.

In Table 2 we compile some basic metadata of the datasets analysed (such as Nrec, M and R range, azimuthal gap), along with all the results of the analyses and assessment presented in this section, namely: f0, A0, f1, A1, SD0.3-30, SD1-10, SDfo, a description of amplification pattern and directional variability, and the cluster from the analysis above. We also make an assessment of site category as per EC8, considering e.g. that class A has f0 > 10 Hz as per the new EC8 draft (Labbe and Paolucci, 2022); class B has f0 above 2-3 Hz; class C lower, etc.). Considering all HVSR characteristics, the final columns provide our judgement about each station's reference potential considering mean and sensitivity separately. GR10 and GR13 seem the best combinations, while GR18 and GR27 seem the worst.

Table 2. Detailed results of the HVSR analysis.

No.	Station code	ML range	Repi range (km)	Depth range (km)	Max AZ gap (deg)	Nrec	f0 (Hz)	A0	f1	A1	SD_f0	SD_1-10	SD_0.3-30
1	GR01	2.0-5.1	9.4-283.9	4.7-16.7	51	44	—	1	—	—	—	1.1	1.17
2	GR02	2.0-5.1	19.9-273.4	3.9-16.7	64	80	—	1	—	—	—	1.18	1.15
3	GR03	2.0-5.1	5.9-289.9	3.9-17.3	163	33	—	1	—	—	—	1.1	1.15
4	GR04	2.0-5.1	14.7-275.6	9.3-17.3	158	26	—	1	—	—	—	1.12	1.14
5	GR05	2.2-3.9	25.7-155.8	7.9-16	147	11	6.4	3.3	—		1.03	1.09	1.08
6	GR06	2.1-4.9	50-224.3	5.6-73	114	20	0.25	3	—	—	1.1	1.1	1.11
7	GR07	2.0-5.1	3.9-263.6	4.6-18.9	59	78	—	1	—	—	—	1.11	1.18
8	GR09	2.0-3.9	10.8-144.7	6.1-17.3	41	82	5.6	5	—	—	1.24	1.12	1.18
9	GR10	2.0-5.1	2.9-318.7	4.7-46.8	40	110	—	1	—	—	—	1.06	1.11
10	GR11	2.0-5.7	12.5-377.8	5.5-81.9	55	73	—	1	—	—	—	1.09	1.09
11	GR12	2.0-5.1	5.7-233.5	4.7-81.9	27	77	0.5-3	1	—	—	1.12	1.12	1.29
12	GR13	2.1-5.7	13.9-389.3	6.1-81.9	29	92	—	1	—	—	—	1.06	1.09
13	GR14	2.5-5.7	10.3-303.4	4.0-46.8	33	94	1.5	2.8	3.8	03	1.19	1.11	1.12
14	GR15	2.5-4.4	23.2-147.2	4.0-81.9	21	146	8.3	5.9	—	—	1.05	1.07	1.08
15	GR16	2.0-5.7	8.7-320.9	5.3-81.9	36	109	2.3	4.4	—	—	1.1	1.09	1.15
16	GR17	2.5-4.9	2.4-220.3	4.6-82.3	31	143	—	1	—	—	—	1.12	1.18
17	GR18	2.5-5.0	38.1-215.3	6.0-81.9	80	96	3	3.1	—	—	1.38	1.17	1.16

No.	Station code	ML range	Repi range (km)	Depth range (km)	Max AZ gap (deg)	Nrec	f0 (Hz)	A0	f1	A1	SD_f0	SD_1-10	SD_0.3-30
18	GR19B	2.0-4.2	7.2-142.7	2.0-46.8	75	190	—	1	—	—	—	1.1	1.12
19	GR20	2.5-5.1	4.5-241.4	5.7-81.9	26	118	16.9	2.7	—	—	1.38	1.08	1.2
20	GR21	2.5-5.1	19.8-235.1	5.7-81.9	46	125	5-8	3.2	—	—	1.21	1.12	1.12
21	GR22	2.5-5.1	20.7-228.8	6.0-122.9	28	124	—	1	—	—	—	1.07	1.08
22	GR23	2.5-5.0	3.2-185.6	6.0-122.9	19	156	0.4-0.7	1	—	—	1.21	1.1	1.11
23	GR24	2.5-5.1	7.1-226.4	5.3-122.9	28	268	7.5	1	—	—	1.29	1.12	1.17
24	GR26	2.5-5.0	1.0-144.6	5.0-122.9	18	187	—	1	—	—	—	1.07	1.09
25	GR27	2.5-5.2	2.0-281.7	5.3-112.4	27	219	1	1	—	—	1.31	1.14	1.14
26	GR28	2.5-5.7	1.8-235.6	4.9-68.8	35	162	—	1	—	—	—	1.14	1.12
27	GR29	2.5-5.1	2.2-185.1	4.6-82.5	17	270	—	1	—	—	—	1.08	1.1
28	GR30	2.5-5.1	5.9-169.8	4.6-122.9	25	158	—	1	—	—	—	1.11	1.15
29	GR31	2.5-5.7	33.0-235.7	4.5-122.9	21	200	—	1	—	—	—	1.12	1.16
30	GR32	2.5-5.7	3.4-215.6	4.6-174.5	19	280	9.6	3.2	—	—	1.1	1.06	1.14
31	GR33	2.5-5.7	21.6-269.2	2.0-112.4	15	263	—	1	—	—	—	1.11	1.1

Table 2. Detailed results of the HVSR analysis (continued).

No.	Station code	Directional variability <10 Hz	Directional variability HF	Cluster no.	Potential EC8 class	Response description (mean HV)	Potential reference site?	
							(directionality)	(mean HV)
1	GR01		high	2	A	flat, near reference	no	yes
2	GR02	high		2	A	flat, near reference	no – avoid	yes
3	GR03			2	A	flat, near reference		yes
4	GR04			2	A	flat, near reference		yes
5	GR05	low	low	3	B	small MF amplification	yes	no
6	GR06			1	A	small HF amplification		no
7	GR07		high	2	A	flat, near reference	no	yes
8	GR09		high	3	B	MF amplification	no	no
9	GR10	very low		4	A	Reference station	preferred	preferred
10	GR11	low	low	2	A	flat, near reference	yes	yes
11	GR12		very high	2	?	small LF broadband amp	no	no
12	GR13	very low	low	4	A	Reference station	preferred	preferred
13	GR14			2	C	small LF amplification		no

No.	Station code	Directional variability <10 Hz	Directional variability HF	Cluster no.	Potential EC8 class	Response description (mean HV)	Potential reference site?	
							(directionality)	(mean HV)
14	GR15	very low	low	1	A/B	HF amplification	preferred	no
15	GR16	low		2	B/C	LF amplification	yes	no
16	GR17		high	4	A	Reference station <15 Hz	no	preferred
17	GR18	high	high	2	B/C	MF amplification	no – avoid	no
18	GR19B			2	A	flat, near reference		yes
19	GR20	low	very high	2	A	Reference station <15 Hz	no	preferred
20	GR21			3	B	broad MF amplification		no
21	GR22	very low	low	2	A	flat, near reference	preferred	yes
22	GR23			2	?	VLF amplification		no
23	GR24		high	3	A/B	HF amplification	no	no
24	GR26	very low	low	2	A	flat, near reference	preferred	yes
25	GR27	high		2	?	small LF broadband amp	no – avoid	no
26	GR28	high		2	?	small LF broadband amp	no	no
27	GR29	low		2	A	flat, near reference	yes	yes
28	GR30			2	A	flat, near reference		yes
29	GR31		high	4	A	flat, near reference	no	yes
30	GR32	very low		1	A	HF amplification	yes	no
31	GR33			4	A	Reference station		preferred

4. Parameters from external sources

In the previous section we computed FAS-based HVSR for the first time for the Greek 1Y Adria Array stations. We studied the results in great detail and used them to assess station reference potential. In this section we compile as many parameters as we can find from external sources, to complete the desk study. The factors that may affect the stations' reference potential and for which we believe we can derive some useful information from external sources in a consistent way across all stations (i.e. not replying on special studies for any of the individual stations but on sources that cover all stations similarly) are: surface geology, topography and slope, housing, and noise.

4.1 Geology

In our study, we compile and carefully study 1:50,000 scale geological maps published for Greece by the Hellenic Survey of Geology and Mineral Exploration (EAGME). We acknowledge that these maps may lack high definition, but they were selected for their consistency and presumed homogeneity across the study area, i.e. the entire country, rather than seeking individual focus studies which would not be available for all stations. Using the information provided in the maps, we compile simplified descriptions of the geological units and their geological

age for each station. In some cases, the geological setting of a station was straightforward to interpret. For example, station GR10 is clearly situated within a granitic formation. In other cases, the interpretation was more complex. Station GR28 (Kastro Kyllinis), for instance, lies in a region generally characterized by marls and clays, but includes a localized occurrence of limestone where this station is located. In Table 3 we compile the information from the maps (formation legend symbol, name of map sheet), our assessments on geological age and unit per station, and our judgement as to station reference potential based on geological characteristics, as we did above for HVSR characteristics.

We note here that other sources can also be found, such as European repositories, which ensure consistency across borders (albeit at the expense of accuracy). This may be useful in future if we attempt to compile AA station geological descriptors across countries, because if only national sources (likely with different scales and with dubious consistency at the borders) are used, consistency will be an issue.

Table 3. Results of the geological desk study based on EAGME geological maps.

No.	Station code	EAGME map	Geological symbol	Geological unit	Geological Age	Potential reference site? (geology)
1	GR01	Neon Petritsion	mr sch	Metamorphic Formations of the Rhodopi Massif: Marbles series	Pliocene – Pleistocene	yes
2	GR02	Drama	mr2	Marbles	Tertiary (most probably Pliocene)	yes
3	GR03	Xanthi	γ1	Igneous rocks (younger granitic rocks)	Oligocene	yes
4	GR04	Abdera-Mesi	Es-Oli.c	Conglomerates with pebbles from metamorphic and granitic rocks	Upper Eocene – Lower Oligocene	no
5	GR05	Maronia Rodopi	θ – θ πγ	Gabbros-Gabbro-diorites & Gabbro-pegmatitic zone: gabbropegmatite veins	Paleocene – Lower Eocene	yes
6	GR06	Didymoteicho	ga	Amphibolites and gneisses	Eocene – Oligocene – Miocene	yes
7	GR07	Edessa	o	Serpentinites	Mesozoic metamorphism	likely yes
8	GR09	Stavros	ab-gn.bi	Amphibolites alternating with biotite gneiss	Paleozoic	yes
9	GR10	Siatista	γ1	Crystaline basement: Granite	Neopaleozoic (most probably Triassic)	yes
10	GR11	Veria	Pti-ii	Old terraces with clays, gravels and conglomerates	Late Pliocene – Pleistocene	no
11	GR12	Katerini	Ms – Pll.st,m	Formations of Aiginio – Katachas (brackish – lacustrine facies): sands, marls, clays and sandstones	Neogene (Upper Miocene – Lower Pliocene)	no
12	GR13	Vasilika	M4 – Pli.I	Red clays series (lacustrine to terrestrial): clays with mica flakes, quartz and lenticular sands, marls, marly limestones and conglomerates	Neogene (Upper Miocene – Lower Pliocene)	no

No.	Station code	EAGME map	Geological symbol	Geological unit	Geological Age	Potential reference site? (geology)
13	GR14	Kalambaka	e – k	Sublithographic limestones along with silex and microbrecciated limestones	Eocene	likely yes
14	GR15	Metsovo	Fo – st	Pindos Zone: Sandstones of Pindos flysch	Eocene	no
15	GR16	Livadero	gs	Metamorphic rocks in the Pelagonian Zone: gneisses, schists, amphibolites	Pre-Alpine Series	yes
16	GR17	Kalambaka	M.mi	Molassic formations of the Hellenic Trough: Upper Meteora Series with gneiss conglomerates, alternating with sandy marls	Oligocene	no
17	GR18	Platykambos	sch.mi	Micaschists	Paleozoic – Middle Triassic	yes
18	GR19B	South Corfu	Pl-mg	Molassic Formations of Southern Corfu: Marls and sandstones	Pliocene	no
19	GR20	Agrafa	K8-9 – k	Pindus Zone: thick bedded Limestones	Upper Cretaceous	yes
20	GR21	Velestino	J? sch	Pelagonian zone: Lower tectonic unit: Schists	Most probably Jurassic	yes
21	GR22	Amliros	TRJ – Dk	dolomites and limestones metamorphic to marbles	Middle Triassic – Jurassic	yes
22	GR23	Istiaia	al	Alluvial deposits	Holocene	no
23	GR24	Lidoriki	ft Es – Oli k.m	Marl – Pelitic Sequence – Transition beds	Upper Eocene – Lower Oligocene	no
24	GR26	Theva	Ts – J9	Dolomites and dolomitic limestones	Upper Triassic	likely yes
25	GR27	Rafina	sch.ab	Neohellenic Tectonic Nappe unit: Tsakeoi schists	Mesozoic	yes
26	GR28	Vartholomio	Jm Ks	Adriatic – Ionian series: thin-bedded up to thick-bedded limestones	Middle Jurassic – upper Cretaceous	yes
27	GR29	Tropaia Arkadias	K8 Pc.k	Pindos Zone: Limestones	Paleocene	yes
28	GR30	Argos	Ks k	Olonos – Pindos series: limestones	Upper Cretaceous	yes
29	GR31	Goritsa	je	Semimetamorphic series of Peloponnese – Crete: Platy limestone series “Plattenkalk”, undivided	Jurassic – Eocene	yes
30	GR32	Molai	sc.cs	Scree and talus cones	Quaternary	no
31	GR33	Xirokampion	Ks – Es .k	Autochonous series, Plattenkalk – Ionian zone: Limestones	Upper Senonian – upper Eocene	yes

4.2 Topography and slope

We extracted the main characteristics of the geomorphology at each site (mainly the ground slope and morphology of the surrounding area) using Google Earth Pro (https://www.google.com/earth/about/versions/). Initially, pins were placed at the exact coordinates that represented each seismological station. To capture key geomorphological features of each site, we generated topographic profiles by drawing paths with the "Add Path" tool, always keeping the station at the center of the profile. Multiple paths were drawn in various directions (e.g. N-S, E-W, NE-SW, NW-SE) in order to extract the profile with the sharpest slope and compute it. We used "Show Elevation Profile" function to obtain elevation data and examine surface morphology.

For the topographic classification of each station, we adopted the scheme proposed in the European Strong-Motion (ESM) database, which is based on average slope values derived from digital elevation models. The four categories of the classification are T1, T2, T3, and T4 (Topographic class T1: 'Flat surface, isolated slopes and cliffs with average angle $i \leq 15°$'; T2: 'Slopes with average angle $i > 15°$'; T3: 'Ridges with crest width significantly less than the base width and average slope angle $15° < i \leq 30°$'; T4: 'Ridges with crest width significantly less than the base width and average slope angle $i > 30°$'). These are aligned with the Italian seismic code (NTC18; Ministero delle infrastrutture e dei transporti, 2018). We also make a different classification, more consistent to Ktenidou et al. (2024): flat (<5°) within 200 m; shallow (<15°) within 200 m; steep (<30°) within 200 m; cliff. This combined methodology allowed us to have a detailed and consistent topographic characterization of each station, integrating visual interpretation with quantitative criteria including definitions from established seismic codes.

To better illustrate the variability in topographic conditions across the network, in Fig. 8 we highlight two stations that exhibit some of the steepest and shallowest slopes respectively. GR20 is located in the mountainous region of Itamos, at an elevation of approximately 800 m, positioned on the hillside of a gorge next to a dam. The maximum local slope reaches 24°, and based on its terrain characteristics, the site is classified as T3 which cannot be used as a reference station. Such topography may induce topographic amplification effects with complex wave fields along the slope due to its steep and complex geometry. In contrast, GR23 is located in Rovies, Evia, in a flat coastal area where the local slope is practically negligible (~2°), representing the minimum slope observed in the network. This site is classified as T1 and, given the minimal influence of topography, serves as an example of an excellent reference station in terms of topography and slope.

It should be mentioned that not all proximity to a topographic feature is equally disadvantageous. It is well known that areas near the crest of a hill or slope suffer from topographic amplification, which makes them poor candidates

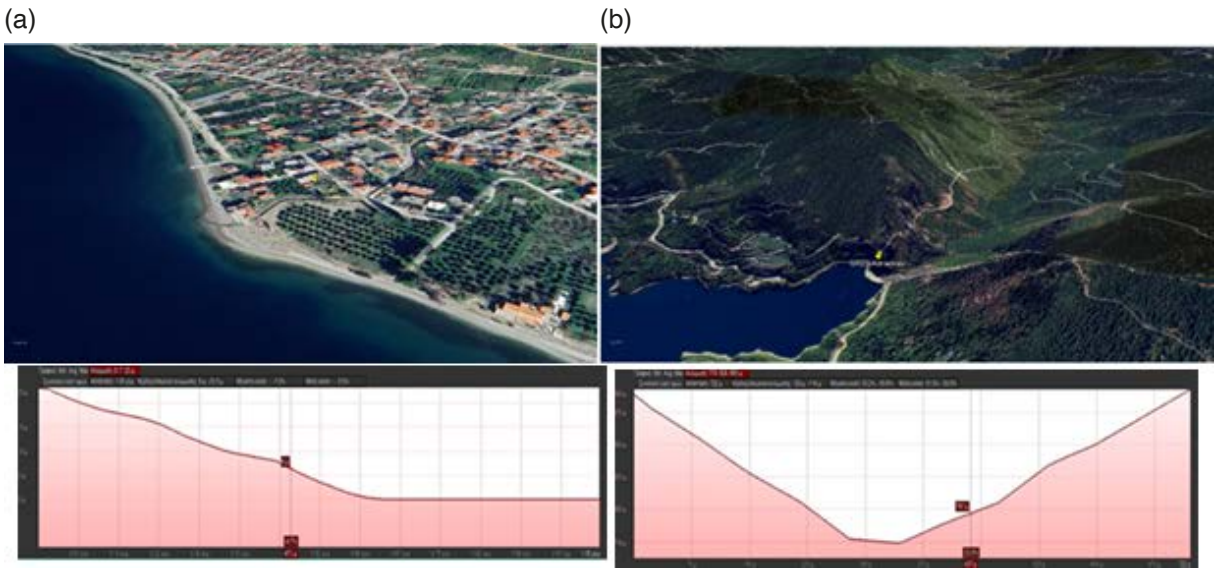

Figure 8. (a) Example of a station on a steep hillside of a gorge, characterised as T3 and hence not an ideal reference site in terms of slope and topography (GR20). (b) Example of a flat seaside region characterised as T1 and hence an acceptable reference site with regards to topography (GR23) Top panels show GoogleEarth 3D views and bottom panels show cross-sections. (Source: Google Earth Pro, https://earth.google.com/intl/earth/versions/#earth-pro, last accessed April 2025).

as reference sites. Locations at the crest of a slope do not amplify (deamplification is sometimes mentioned but is not very well substantiated) and so would be more acceptable candidates. Locations along the slope exhibit strong fluctuations of ground motion and variability, making them poor candidates. The best locations would lie several dozens of meters far from a topographic anomaly and especially its crest.

Table 4 compiles all information and assessments from our desk study related to topography. Data include elevation, estimated slope using GoogleEarthPro in % and degrees, concise characterisation of topographic category as per ESM (T1-T4) and for the 200 m around the station, more detailed comment after extensive study of the 3D terrain, and our judgement of reference station capacity.

Table 4. Results on topography and slopes from the desk study based on Google Earth and Google Maps.

No.	Station code	Station Elevation (m)	Slope (%) from GoogleEarth	Slope (Degrees)	Topography assessment	Topography code (ESM)	Additional comments on topography	Potential reference site? (topography)
1	GR01	219	29%	16	steep (<30°) within 200 m	T1	at the bottom of a small valley, between two hills	no
2	GR02	238	38%	21	steep (<30°) within 200 m	T2	slightly above the toe of a hill	likely
3	GR03	296	33%	18	steep (<30°) within 200 m	T2	castle near monastery – top of small hill	no
4	GR04	143	18%	10	shallow (<15°) within 200 m	T1	on a hill plateau near crest	likely
5	GR05	69	12%	7	shallow (<15°) within 200 m	T1	base of a shallow slope	yes
6	GR06	277	7%	4	flat (<5°) within 200 m	T1	flat	yes
7	GR07	506	20%	11	shallow (<15°) within 200 m	T1	on a geltne hillside	yes
8	GR09	80	25%	14	shallow (<15°) within 200 m	T1	on a small plateau, maybe an old quarry with landfill	likely*
9	GR10	781	14%	8	shallow (<15°) within 200 m	T1	In a small valley with hills around	yes
10	GR11	300	24%	13	shallow (<15°) within 200 m	T1	near the top pf a very mild hill	likely
11	GR12	130	18%	10	shallow (<15°) within 200 m	T1	near top of a small mild slope	likely
12	GR13	300	15%	9	shallow (<15°) within 200 m	T1	very gentle slopes	yes
13	GR14	570	21%	12	shallow (<15°) within 200 m	T1	top of gentle hill	likely
14	GR15	1016	36%	20	steep (<30°) within 200 m	T3	near the bottom of a gorge	likely
15	GR16	1101	24%	14	shallow (<15°) within 200 m	T1	on a hilltop, gentle slopes	likely

No.	Station code	Station Elevation (m)	Slope (%) from GoogleEarth	Slope (Degrees)	Topography assessment	Topography code (ESM)	Additional comments on topography	Potential reference site? (topography)
16	GR17	493	—	—	cliff	T4	on a vertical cliff	no
17	GR18	1031	32%	18	steep (<30°) within 200 m	T2	near top of mountain plateau	no?
18	GR19B	114	23%	13	shallow (<15°) within 200 m	T1	gentle slopes	yes
19	GR20	836	45%	24	steep (<30°) within 200 m	T3	steep hillside of a gorge	no
20	GR21	366	16%	9	shallow (<15°) within 200 m	T1	almost horizontal plain	yes
21	GR22	333	20%	11	shallow (<15°) within 200 m	T1	top of a gentle hill	likely
22	GR23	67	3%	2	flat (<5°) within 200 m	T1	flat, seaside	yes
23	GR24	893	42%	23	steep (<30°) within 200 m	T3	on a mountainous slope	no
24	GR26	782	75%	37	steep (<30°) within 200 m	T4	top of steep cliff	no
25	GR27	105	20%	11	shallow (<15°) within 200 m	T1	on a gentle hillside	likely
26	GR28	236	31%	17	steep (<30°) within 200 m	T2	on a rocky hill, castle	no
27	GR29	630	19%	11	shallow (<15°) within 200 m	T1	on a gentle hillside	yes
28	GR30	483	41%	22	steep (<30°) within 200 m	T3	near toe of a hill	likely
29	GR31	379	13%	7	shallow (<15°) within 200 m	T1	toe of a very mild slope	yes
30	GR32	75	35%	19	steep (<30°) within 200 m	T2	base of a hill	likely
31	GR33	424	28%	16	steep (<30°) within 200 m	T2	on a slope of a rocky mountain range	no

4.3 Housing

While evaluating the topography and slopes for each station, we also examined the housing conditions at the 1Y AdriaArray stations. Almost all stations are in some kind of structure, and we extracted from GoogleEarth and GoogleMaps street view the geometry (number of floors and footprint area) as well as some assessments of the type of building and an idea of its age. In most cases, the buildings have only the ground floor and only 2 had a second storey. We calculated the height and footprint based on the perceived dimensions in the google map photographs. All the available information about the housing is shown in Table 5 we compile information on the type and age of buildings, the number of storeys and our assessment as to whether each station can be considered as reference or not. Figure 9 shows, from left to right, some indicative cases: a stone-built structure with a tiled roof in Doliana,

which houses the GR14 station; a historic stone monastery with a tiled roof, where the GR17 station is located; and a small concrete structure housing GR20. Table 5 compiles information gathered from image and map inspection relating to the structure's geometry, but also to the degree possible comments are given as to its potential use, material, age, general description, etc. The general description (free text) includes a symbol that indicates how many free sides the structure has, e.g. 4f for the typical case of a free-standing structure, and less if it is in direct contact with another one on 1, 2 or more sides.

Figure 9. Examples of the variability in housing conditions: from left to right, stations GR14, GR17 and GR20 (Source: Google Maps, https://www.google.gr/maps/, last accessed April 2025).

Table 1. Table 5. Results on station housing characteristics from the desk study based on Google Earth and Google Maps.

No.	Station code	Type of Building	Number of storeys above ground floor	Height (m)	Footprint (m^2)	Building Age
1	GR01	Little outhouse with concrete roof (or a little church), 4f	0	3	25	
2	GR02	little house with a tiled roof, 4f	0	3	96	
3	GR03	outhouse with a concreted roof, 4f	0	3	200	
4	GR04	Little church of Agios Athanasios with a tiled roof, 4f	0	3	72	
5	GR05	metal military archy toll inside a campus, 4f	0	4	48	old
6	GR06	house with a tiled roof, 4f	0	3	104	
7	GR07	Little outhouse with a tiled roof, 4f	0	3	72	new
8	GR09	Little warehouse with a metal roof, 4f	0	3	32	new
9	GR10	little house with a tiled roof, 4f	0	3	120	new
10	GR11	house with a tiled roof, 4f	0	3	180	
11	GR12	Concrete warehouse	0	3	224	
12	GR13	house with a tiled roof, 4f	0	3	150	new
13	GR14	Elementary School or Health Center constructed with stone-style with tiled roof, 4f	0	3	420	old

No.	Station code	Type of Building	Number of storeys above ground floor	Height (m)	Footprint (m^2)	Building Age
14	GR15	Community office constructed with tiled roof and backfilled basement, 4f	0	4	192	old
15	GR16	church with a tiled roof, 4f	0	4	156	
16	GR17	very old stone constructed monastery with tiled roof, 1f	1	6	32	very old
17	GR18	metal roof which are installed solar panels, 4f	0	3	250	new
18	GR19B	an old outhouse close to a small church into the forest, 4f	0	3	120	old
19	GR20	small outhouse with tiled roof, 4f	0	3	12	old
20	GR21	small church close to cemetery with tiled roof, 4f	0	3	136	old
21	GR22	small warehouse with tiled roof, 4f	1	6	84	new
22	GR23	a house with tiled roof, 4f	0	3	70	new
23	GR24	Community office constructed with stone-style with tiled roof, 4f	0	3	168	new
24	GR26	R/C building with slab roof, 4f	0	4	64	new
25	GR27	warehouse with tiled roof, 4f	0	3	15	old
26	GR28	old warehouse with tiled roof, 4f	0	3	60	old
27	GR29	large and long building, most probably old school, with tiled roof, 4f	0	3	192	old
28	GR30	R/C building with slab roof, 4f	0	3	300	new
29	GR31	old elementary school of a small village with tiled roof, 4f	0	3	486	old
30	GR32	large old elementary school far away from a small village with tiled roof, 4f	0	5	336	old
31	GR33	small outhouse with concrete roof, 4f	0	3	9	old

4.4 Noise

Following the desk study assessment of topography and housing conditions, we finally attempted to evaluate the potential for high noise levels at each site, based solely on the inspection of maps. Considering factors such as accessibility (based on vegetation, terrain and transport networks), proximity to roads, land use, population and touristic value of village/town, and proximity to water bodies such as the sea or rivers, we roughly evaluated the potential noise levels at each site based on its location and surrounding environment. For instance, stations situated within buildings in populated village areas, near main roads or water etc., were classified as potentially noisy,

while those located in more isolated places were considered as quiet. In Table 6 we compile all the noise-related information we collected and characterise each station as potential reference or not based on our observations. We note that this is a very tentative approach that can be viewed in conjunction with the routine SOH (state-of-health) metrics provided by the operators, which include noise monitoring. Such data are already provided by the agencies (https://bbnet.gein.noa.gr/HL/1y and https://www.geophysik.ruhr-uni-bochum.de/adriaarray/soh.html). These data include average noise levels for different periods (current month, current year, and entire period of operation) compared to the global noise model proposed by Peterson (1993). For the Greek 1Y stations, we found some correlation to our observations, but this would require further study. We note here that we do not make mention to noise level in terms of monitoring and detection capability per se, but overall quality of recorded signal for engineering seismology applications.

Table 6. Results on potential noise characteristics from the desk study based on Google Earth and Google Maps.

No.	Station code	Station name	Additional comments on potential noise	Potential reference site? (noise)
1	GR01	Neo Petritsi, Serres	quiet	yes
2	GR02	Drama	quiet, outside city	yes
3	GR03	Xanthi	quiet, near monastery	yes
4	GR04	Abdera	quiet, park	yes
5	GR05	Maronia-Sapes, Petrota	close to the sea and a new highway construction site	no
6	GR06	Mavrokklisi	in a small village	yes
7	GR07	Mesimeri, Edessa	in a monastery area	yes
8	GR09	Rentina	near a village football field	yes
9	GR10	Kriovrisi, Ptolemaida	in a small village, quiet	yes
10	GR11	Veroia	quiet, in a monastery area	yes
11	GR12	Katachas	quiet	yes
12	GR13	Katsika, Petralona	quiet	yes
13	GR14	Doliana	In a large village, near main road	no
14	GR15	Vouvousa	near a flowing stream, small village	no
15	GR16	Livadero	quiet	yes
16	GR17	Meteora, Kalambaka	inside monastery on cliff	likely
17	GR18	Lakeria	quiet	yes
18	GR19B	Vitalades, Lefkimmi	church in forest, quiet	yes

No.	Station code	Station name	Additional comments on potential noise	Potential reference site? (noise)
19	GR20	Itamos	on road, crest of Plastiras Dam	no
20	GR21	Thetidio	farmland	yes
21	GR22	Monastery Panagia Xenia, Sourpi	in a monastery area (mildly touristic area)	likely
22	GR23	Rovies	very close to the sea, touristic	no
23	GR24	Mousounitsa	quiet	yes
24	GR26	Sagmata Monastery, Theva	quiet monastery, but near windfarm (likely windy)	likely
25	GR27	Kouvelles, Euboea	cemetery area of a small village	yes
26	GR28	Kastro	inside a touristic monument (castle)	no
27	GR29	Doxa	close to the main road of a village	likely
28	GR30	Achladokambos	at the edge of a small village, churchyard	yes
29	GR31	Kephalas	at the edge of a small village, quiet	yes
30	GR32	Zarakas	cross-section of two streams, near main road, sea nearby	no
31	GR33	Lefktro	windy, near road but very remote	likely

To make further use of seismic noise in this work and also considering the fact that in less seismically active areas it may be difficult to collect enough strong-motion data to perform HVSR, we calculated HVSR applied to ambient noise. A full description of the method's basis is out of the scope of this paper, but some seminal references include Nogoshi and Igarashi (1971), Ohta (1963), and Nakamura (1989; 2000). We used continuous recordings of 24-hour duration and extracted multiple 30-min windows across different days/hours. All data were downloaded from the EIDA@NOA node (Evangelidis et al., 2021). We followed guidelines provided by project SESAME (2004). Pre-processing included demeaning, detrending and tapering as appropriate. The 30-min windows were used with a 50% overlap. After Fourier transform computation, smoothing was applied to the spectra as per Konno and Ohmachi, 1998. For every window we computed H/V as the geometric mean of the E and N horizontals divided by Z. Windows failing quality control were rejected. Daily log-averaged medians (±1 SD) of the accepted H/V curves provided station-specific estimates of the site transfer function. Processing was performed with the open-source Python package hvsrpy (Vantassel, 2020; Cox et al., 2020) in the framework of obspy (Beyreuther et al., 2010; Krischer et al., 2015). We computed mean, direction-independent HVSR to assess overall amplification patterns and also component-specific ratios on the E and N components.

We then compared HVSR curves derived from noise recordings with those obtained from earthquake data. By applying the HVSR method to both noise and seismic recordings, we can test whether the background noise excites the same resonant frequencies as seismic waves. Figures 10 and 11 present mean, direction-independent HVSRs for selected stations derived from noise and seismic data. As illustrated in Fig. 10, some stations such as GR07, GR17, GR22, and GR26 show good agreement between the noise and the seismic HVSR over most of the frequency range, with similar overall shapes. Moreover, these stations exhibit nearly flat HVSRs – consistent with their characterization as good reference sites. In Fig. 11 stations GR06, GR09, GR15, and GR32 are presented

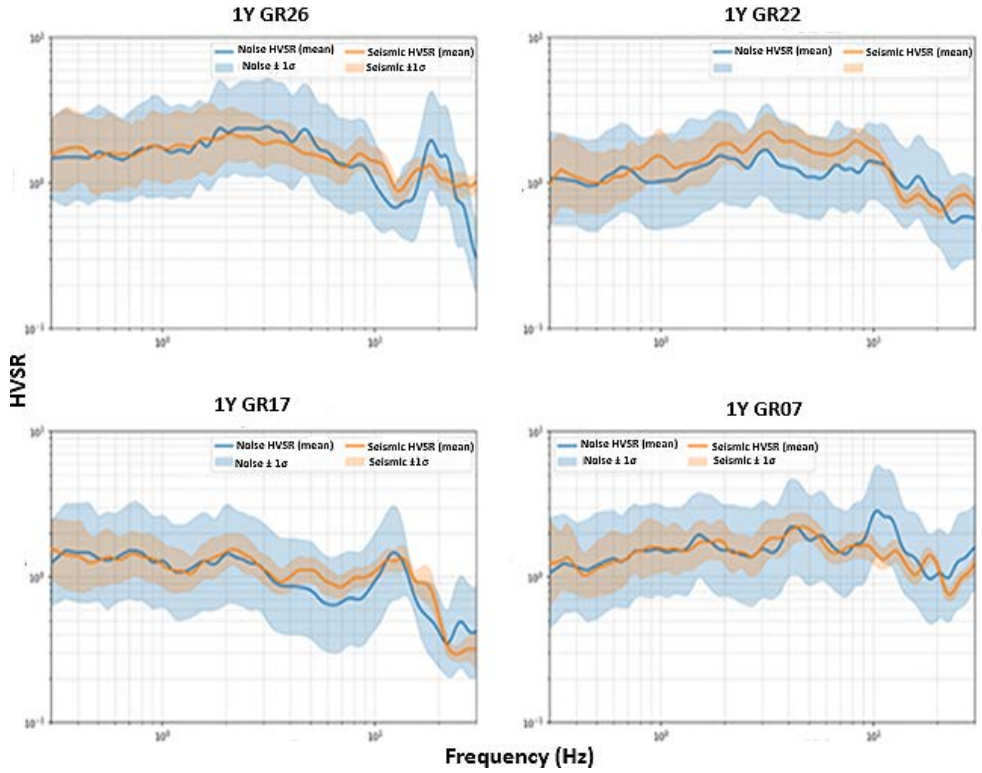

Figure 10. Comparison of horizontal-to-vertical spectral ratios (HVSR) derived from continuous noise (blue) and from earthquake recordings (orange) for selected 1Y stations. Top panels (GR26, GR22, GR17, GR07) illustrate cases where both datasets show flat, near-unity responses consistent with reference-site behavior.

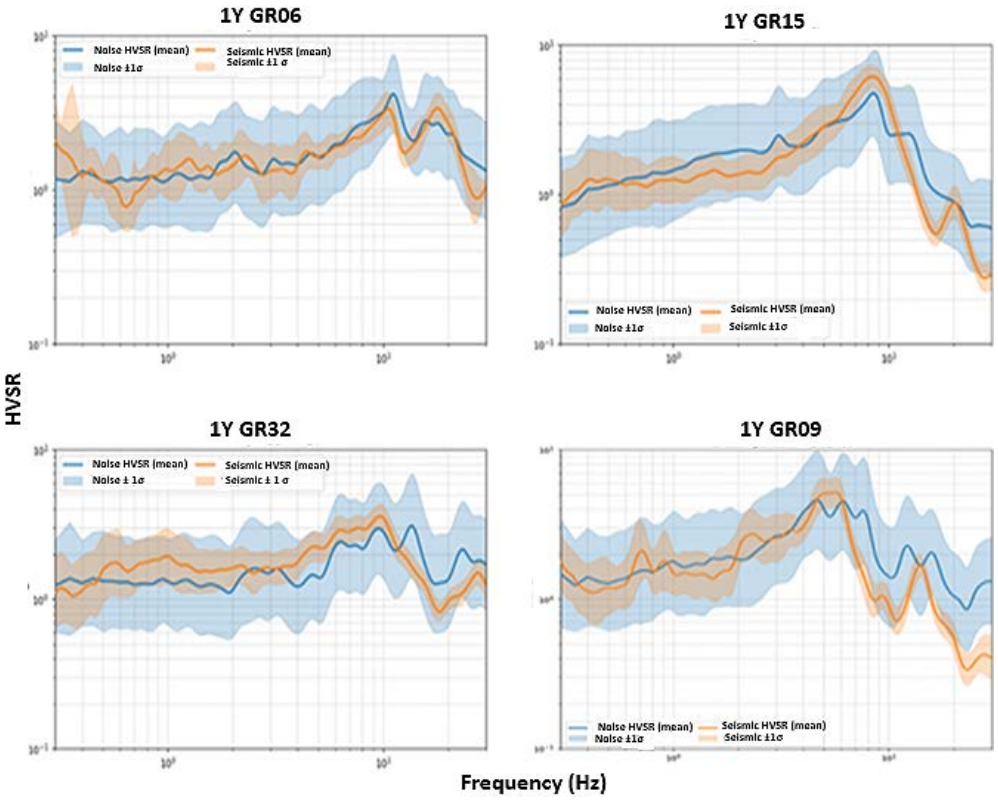

Figure 11. Comparison of horizontal-to-vertical spectral ratios (HVSR) derived from continuous noise (blue) and from earthquake recordings (orange) for selected 1Y stations. Top panels (GR26, GR22, GR17, GR07) illustrate cases where both datasets show flat, near-unity responses consistent with reference-site behavior.

showing satisfying agreement between noise and seismic HVSRs but the observed peaks correspond to significant amplification and thus do not show reference site behavior.

Figure 12 shows that directionality can sometimes also be captured by noise HVSR, in a similar way as by earthquake HVSR (this plot can be compared to Fig. A3 where HVSR was derived from 87 events for station 1Y.GR09 and at the second peak around 12-13 Hz. In the latter, the scatter due to the rotations in the components is large and it is clear that amplitude is 2.5 times higher in the direction of N0-N10 with respect to N90-N100, which is surprisingly consistent with the results in Fig. 12, where the N component of noise causes a peak 2.5 times higher than the E component.

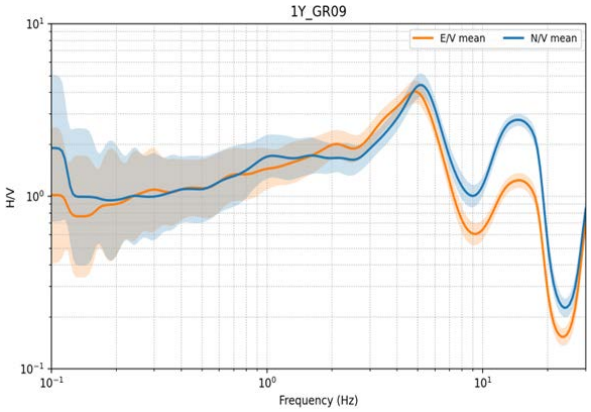

Figure 12. Directionality of horizontal-to-vertical spectral ratios (HVSR) derived from continuous noise in the E (orange) compared to the N component (blue) for station 1Y.GR09.

5. Co-assessing all data to characterise overall reference capacity

In the previous sections, we derived parameters from the waveform analysis, we collected geological information (age, unit) from geological maps, we described housing and noise conditions and we calculated topographic slopes in a preliminary way from Google Earth. The next step is to compile all the available information for each station, consider and weigh it into a final suggestion. Until now, we have characterized the stations as reference or not, based on the mean HVSR results and their directionality, the geology, the topography, the housing and noise conditions separately. In this section we attempt a combined characterisation of the stations, taking into account all the existing parameters. We do not aim to give numerical grading or ordering, as we think this would lack meaning and mathematical basis. We wish to offer a qualitative but weighed and informed overall assessment based on all available information so far.

In Fig. 13 we present all 31 stations and use a schematic colour code to categorise them as good reference candidates (dark blue), likely/possible references (light blue) and inadequate/not reference (red) based on the three main criteria, namely the geology (triangles), the HVSR results (circles) and the topography (dots), overlaying them together to offer an easy visual overview of the stations across the country. By simple inspection it is easy to spot some of the stations that satisfy most criteria (e.g. GR10, GR22, GR30, GR31) vs those that do not (e.g. GR12, GR15, GR24, GR32).

From our waveform analysis, we concluded that 5 stations are clearly flat and considered as reference, 16 exhibited nearly flat responses and the remaining 10 show non-negligible to strong amplification at frequencies below those expected by rock sites (>10 Hz). We note that in this final assessment, the mean shape and directional sensitivity of HVSR is co-assessed, but always giving priority to the shape of the mean: an excellent mean (flat and near-unity) HVSR is the main desired feature and will only become somewhat less appealing if it has high SD values; whereas a very sharp amplitude peak with extremely low SD is still an overall undesired feature.

Table 7 gathers all assessments so far and offers a final disposition per station. Overall, the most complete and adequate reference stations from almost all points of view considered in this paper seem to be sites GR10, GR22 and GR29, marked in the last column of Table 7 as ‘preferred’. On the other hand, the least adequate reference

stations seem to be: GR12, GR13, GR14, GR16, GR17, GR20, GR23, GR24, GR28, GR32. These sites have been underlined in the table. However, this is of course a combination of all possible features and assessments: the user may decide for themselves based on the specific use they intend to make of their data which are key to them. This is why we propose this holistic, transparent scheme for compiling all primary information, so as to facilitate users with prioritising and assessing what is most important to them.

Several cases have both strong advantages and disadvantages, and some exhibited unexpected results. Considering the mean HVSR and its directional variability, station 1Y.GR10 is the best reference candidate, with no significant amplitude in the 0.2-10 Hz frequency band and very low directional variability. From a geological perspective, it is situated on a Neopaleozoic granite formation, which supports its classification as a very good reference site. On the other hand, one of the least satisfactory reference candidates based on HVSR is the 1Y.GR09 station which exhibits strong amplitude at merely 5 Hz (indicating a B EC8 class site, e.g. softer than rock) and high directional variability. It is intriguing that 1Y.GR09 is, based on the geological formation, located on Paleozoic amphibolites alternating with biotite gneiss which would be typically considered as good reference conditions.

Table 7. Compilation of assessment of reference site potential according to all criteria in this study.

No.	Station code	Station name	Geological unit and age	Topography	Noise potential	HVSR shape	HVSR directionality	Overall assessment
1	GR01	Neo Petritsi, Serres	yes	no	yes	yes	no	
2	GR02	Drama	yes	likely	yes	yes	no – avoid	yes
3	GR03	Xanthi	yes	no	yes	yes		
4	GR04	Abdera	no	likely	yes	yes		
5	GR05	Maronia-Sapes, Petrota	yes	yes	no	no	yes	
6	GR06	Mavrokklisi	yes	yes	yes	no		
7	GR07	Mesimeri, Edessa	likely yes	yes	yes	yes	no	yes
8	GR09	Rentina	yes	likely*	yes	no	no	
9	GR10	Kriovrisi, Ptolemaida	yes	yes	yes	preferred	preferred	preferred
10	GR11	Veroia	no	likely	yes	yes	yes	yes
11	GR12	Katachas	no	likely	yes	no	no	no
12	GR13	Katsika, Petralona	no	yes	yes	preferred	preferred	yes
13	GR14	Doliana	likely yes	likely	no	no		no
14	GR15	Vouvousa	no	likely	no	no	preferred	no
15	GR16	Livadero	yes	likely	yes	no	yes	yes
16	GR17	Meteora, Kalambaka	no	no	likely	preferred	no	no
17	GR18	Lakeria	yes	no?	yes	no	no – avoid	no
18	GR19B	Vitalades, Lefkimmi	no	yes	yes	yes		
19	GR20	Itamos	yes	no	no	preferred	no	no
20	GR21	Thetidio	yes	yes	yes	no		
21	GR22	Monastery Panagia Xenia, Sourpi	yes	likely	likely	yes	preferred	preferred

No.	Station code	Station name	Geological unit and age	Topography	Noise potential	HVSR shape	HVSR directionality	Overall assessment
22	GR23	Rovies	no	yes	no	no		no
23	GR24	Mousounitsa	no	no	yes	no	no	no
24	GR26	Sagmata Monastery, Theva	likely yes	no	likely	yes	preferred	yes
25	GR27	Kouvelles, Euboea	yes	likely	yes	no	no – avoid	
26	GR28	Kastro	yes	no	no	no	no	no
27	GR29	Doxa	yes	yes	likely	yes	yes	preferred
28	GR30	Achladokambos	yes	likely	yes	yes		yes
29	GR31	Kephalas	yes	yes	yes	yes	no	yes
30	GR32	Zarakas	no	likely	no	no	yes	no
31	GR33	Lefktro	yes	no	likely	preferred		

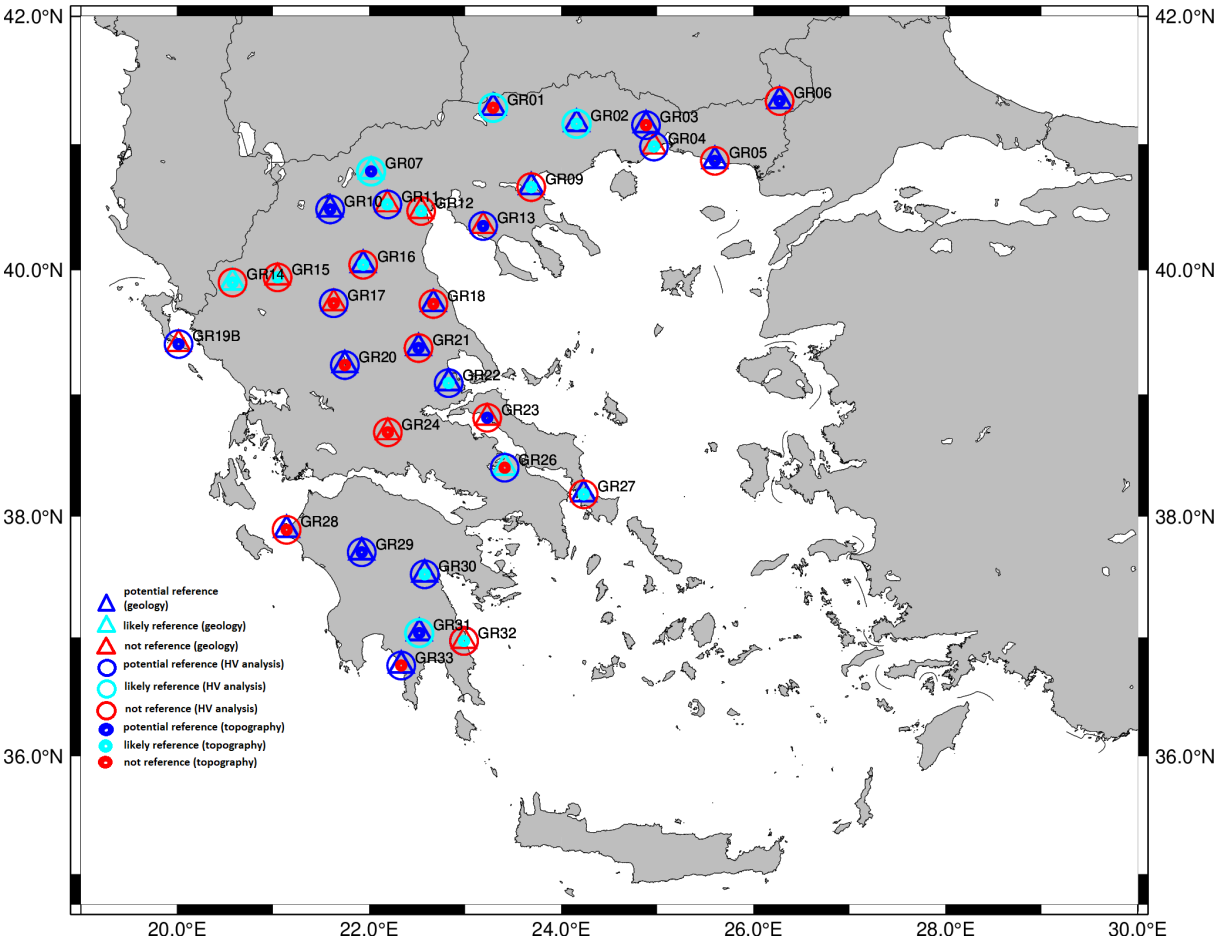

Figure 13. Assessment of reference potential for Greek 1Y stations based on the main criteria investigated here: geology (triangles), HV analysis (circles) and topography (small dots). Reference potential is colour coded, ranging from dark blue for good, light blue for possible, and red for inadequate.

6. Discussion and conclusion

This study aims at compiling available metadata for the 1Y AdriaArray network in Greece. We first created a weak- and strong-motion dataset, carefully curating and processing it. We performed HVSR and compiled waveform-derived parameters from our analysis (f0, A0, SDf0 etc.) and attempted an initial characterisation of stations as reference or non-reference based on the HVSR characteristics. We then collected geological data from geological maps published for Greece by the Hellenic Survey of Geology and Mineral Exploration (EAGME) and classified the stations' reference potential based on those. We then continued the desk study describing the topography/slope, housing conditions and potential noise sources for each site using Google Earth Pro. Moreover, we calculated HVSR of ambient noise and compared our results with the HVSR curves obtained by applying the method at seismic data. Also, we assessed their reliability as reference stations based on those indications. To conclude, we combined the reference characterization of each station for all criteria and made an overall assessment of their potential capacity.

This scheme is open, transparent and reproducible, allowing the user full access to all the building blocks (i.e. parameters and criteria) used, so that s/he can select those most pertinent to her/him. We believe that this scheme, derived so far merely from a desk study, can become more holistic and complete by adding the invaluable observations of the operators, those who have been on site and witnessed all conditions first hand. This is why, in future, we intend to enrich our AdriaArray flatfile with more metadata, compiling additional information about the installation conditions and topography/slope assessment from the operators' site visits, as many photographs as possible from the site, as well as additional geological descriptions both from operators' visits (for more site-specific detail) but also from European harmonized maps (for more compatibility between countries, preparing us for a unified effort across borders among AdriaArray agencies). For Greece, the next step in this work is a close collaboration between NOA and the University of Patras (HP), the National and Kapodistrian University of Athens (NKUA) and the Aristotle University of Thessaloniki (AUTH) to support data collection efforts from all network operators. From the desk study aspect, additional parameters can be considered, such as obtaining Vs30 from geology/slope proxies and data, Vsz profile to a certain depth from P-wave polarization (e.g. Kim et al., 2016) and the high-frequency attenuation factor $\kappa 0$ (Anderson and Hough, 1984; Ktenidou et al., 2014) from earthquake data. If budget were a priori available, a variety of in-situ tests could be envisioned, both intrusive and non-intrusive, geotechnical and geophysical, but this is not the case here and for this reason we do not consider any method that requires mobilisation and equipment. Discussions are underway within AdriaArray regarding how best to collect and combine such data, considering – and potentially expanding – existing FAIR tools such as the ORFEUS EIDA Station Book (https://orfeus-eu.org/stationbook) or other options.

We hope this article will inspire more countries and agencies deploying AdriaArray stations to turn a scrutinising eye towards station conditions. Finally, we would like to emphasize the importance and urgency we see in collecting field observations, particularly due to the array's partially temporary nature. There is a last chance for all operators to collect photographic documentation and detailed descriptions before any more temporary stations are dismantled, and we hope this work will help convince them of the importance of such an effort. Desk studies can then follow at leisure, and the final product can be combined to ensure a much more consistent characterisation of stations throughout this big endeavour that is AdriaArray.

Acknowledgements. Access to full waveform data from AdriaArray 1Y network is possible through ORFEUS EIDA, and specifically through the EIDA@NOA node (https://doi.org/10.7914/y0t2-3b67). Data from temporary stations such as network code 1Y are initially accessible to the AdriaArray Seismology Group participants and then open subject to a rolling 2-year embargo. EAGME maps are generally available for purchase, and more information is available here: https://www.eagme.gr/. Some plots were made using GMT (Wessel et al., 2019), https://www.generic-mapping-tools.org/ and we gratefully acknowledge this great tool. GoogleEarth was used to inspect stations remotely (http://www.google.com/earth/index.html; last accessed April 2025). Freely accessible code hvsrpy (Vantassel, 2020; Cox et al., 2020) in the framework of obspy (Beyreuther et al., 2010; Krischer et al., 2015) is gratefully acknowledged. We acknowledge discussions within AdriaArray, including coordinators Petr Kolínský and Thomas Meier, Engineering Seismology Collaborative Research Group co-leads Costas Papazachos and Iva Dasovic, and Greek network operators Christos Evangelidis, Efthimios Sokos and George Kaviris. Discussions on noise HVSR with John Ebel and Francisco-Jose Chávez-García were very helpful to us and deserve a special thank you. Finally, we would like to cordially thank the

Editor and two anonymous reviewers for their kind and valuable suggestions which improved the presentation and impact of this work. Analysis of stations in Macedonia and Thrace is co-funded by EU project COREU, with funding from the European Union's HE research and innovation programme under grant agreement No 101136217.

References

Anderson, J. G. and S. E. Hough (1984). A model for the shape of the Fourier amplitude spectrum of acceleration at high frequencies, Bull. Seismol. Soc. Am., 74, 1969-1993, doi:10.1785/BSSA0740051969.

Beyreuther, M., R. Barsch, L. Krischer, T. Megies et al. (2010). ObsPy: A Python toolbox for seismology, Seismol. Res. Lett., 81, 3, 530-533, doi:10.1785/gssrl.81.3.530.

Brune, J. N. (1970). Tectonic stress and the spectra of seismic shear waves from earthquakes, J. Geoph. Res., 75, 26, 4997-5002, doi:10.1029/JB075i026p04997.

Brune, J. N. (1971). Correction to Tectonic stress and the spectra of seismic shear waves from earthquakes, J. Geoph. Res., 76, 20, 5002, doi:10.1029/JB076i020p05002.

Cox, B. R., T. Cheng, J. P. Vantassel and L. Manuel (2020). A statistical representation and frequency-domain window-rejection algorithm for single-station HVSR measurements, Geophys. J. Int., 221, 3, 2170-2183, doi:10.1093/gji/ggaa119.

CEN – Comité Européen de Normalisation (2004). Eurocode 8: Design of structures for earthquake resistance. Part 1: general rules, seismic actions and rules for buildings, EN 1998-1, 2004, Brussels, Belgium, TS30.

Cultrera, G., C. Cornou, G. Di Giulio and P. Y. Bard (2021). Indicators for site characterization at seismic station: recommendation from a dedicated survey, Bull. Earthquake Eng. 19, 2, 4171-4195, doi:10.1007/s10518-021-01136-7.

Di Giulio, G., G. Cultrera, C. Cornou, P. Y. Bard et al. (2021). Quality assessment for site characterization at seismic stations, Bull. Earth. Eng., 19, 12, 4643-4691, doi:10.1007/s10518-021-01137-6.

Evangelidis, C. P., N. Triantafyllis, M. Samios, K. Boukouras et al. (2021). Seismic waveform data from Greece and Cyprus: Integration, archival and open access, Seismol. Res. Lett., 92, 1672-1684, doi:10.1785/0220200408.

Friederich, W., C. Evangelidis, C. Papazachos, E. Sokos et al. (2022). AdriaArray Temporary Network: Greece, North Macedonia, Data set, International Federation of Digital Seismograph Networks, doi:10.7914/y0t2-3b67.

Goulet, C. A., Y. Bozorgnia, N. M. Kuehn, L. Al Atik et al. (2021). NGA-East Ground-Motion Characterization model part I: Summary of products and model development, Earthq. Spectra, 37, 1, 1231-1282, doi:10.1177/87552930211018723.

Kim, B., Y. M. A. Hashash, E. M. Rathje, J. P. Stewart et al. (2016). Subsurface shear wave velocity characterization using P-wave seismograms in central and Eastern North America, Earthq. Spectra, 32, 1, 143-169, doi:10.1193/123013EQS299M.

Kishida, T., O. J. Ktenidou, R. Darragh and W. Silva (2016). Semi-automated procedure for windowing time series and computing Fourier amplitude spectra (FAS) for the NGA-West2 database, Pacific Earthquake Engineering Research Center, PEER report 2016, 02, 63.

Kolínský, P., T. Meier, M. R. Agius, A. Bijedić et al. (2025). AdriaArray – a Passive Seismic experiment to Study Structure, Geodynamics and Geohazards of the Adriatic Plate, Ann. Geophys., 68, 5, DM555, 2025; doi:10.4401/ag-9284.

Konno, K. and T. Ohmachi (1998). Ground-motion characteristics estimated from spectral ratio between horizontal and vertical components of microtremor, Bull. Seismol. Soc. Am., 88, 1, 228-241, doi:10.1785/BSSA0880010228.

Ktenidou, O. J., F. J. Chavez-Garcia and K. Pitilakis (2011). Variance Reduction and Signal-to-Noise Ratio: Reducing Uncertainty in Spectral Ratios, Bull. Seismol. Soc. Am., 101, 2, 619-634, doi:10.1785/0120100036.

Ktenidou, O. J., F. Cotton, N. Abrahamson and J. G. Anderson (2014). Taxonomy of kappa: A review of definitions and estimation methods targeted to applications, Seismol. Res. Lett., 85, 135-146, doi:10.1785/0220130027.

Ktenidou, O. J., F. J. Chávez-García, D. Raptakis and K. D. Pitilakis (2016). Directional dependence of site effects observed near a basin edge at Aegion, Greece, Bull. Earth. Eng., 14, 3,623-645, doi:10.1007/s10518-015-9843-x.

Ktenidou, O. J. and N. Abrahamson (2016). Empirical estimation of high-frequency ground motion on hard rock, Seismol. Res. Lett., 87, 6, 1465-1478, doi:10.1785/0220160075.

Ktenidou, O. J., N. Abrahamson, W. Silva, R. Darragh et al. (2021). The search for hard-rock kappa (κ) in NGA-East: A semi-automated methodology to estimate κ for large challenging datasets in stable continental regions, Earthq. Spectra, 37, 1391-1419, doi:10.1177/87552930211019763.

Ktenidou, O. J., E. V. Pikoulis, A. Papageorgiou, F. Gkika et al. (2024). The quest for reference stations at the National Observatory of Athens, Greece, Nat. Hazards Earth Syst. Sci., doi:10.5194/nhess-2023-233.

Labbé, P. and R. Paolucci (2022). Developments Relating to Seismic Action in the Eurocode 8 of Next Generation, Progresses in European Earthquake Engineering and Seismology – Third European Conference on Earthquake Engineering and Seismology – Bucharest, 2022, in Collection Springer Proc. Earth Environ. Sci. Radu Vacareanu and Constantin Ionescu (Eds.), Springer, Cham, 26-46, ISSN:2524-342X.

Lanzano, G., C. Felicetta, F. Pacor, D. Spallarossa et al. (2020). Methodology to identify the reference rock sites in regions of medium-to-high seismicity: An application in Central Italy, Geophys. J. Int., 222, 3, 2053-2067, doi:10.1093/gji/ggaS261.

Lanzano, G., L. Luzi, C. Cauzzi, J. Bienkowski et al. (2021). Accessing European Strong-Motion Data: An Update on ORFEUS Coordinated Services, Seismol. Res. Lett., 92, 3, 1642-1658, doi:10.1785/0220200398.

Lermo, J. and F. G. Chávez-García (1993). Site effect evaluation using spectral ratios with only one station, Bull. Seismol. Soc. Am., 83, 5, 1574-1594, doi:10.1785/BSSA0830051574.

Luzi, L., R. Puglia, E. Russo, M. D'Amico et al. (2016). The engineering strong motion database: A platform to access pan-European accelerometric data, Seismol. Res. Lett., 87, 4, 987-997, doi:10.1785/0220150278.

Luzi, L., G. Lanzano, C. Felicetta, M. C. D'Amico et al. (2020). Engineering Strong Motion Database, ESM, Version 2.0, Istituto Nazionale di Geofisica e Vulcanologia-INGV, doi:10.13127/ESM.2.

Ministero delle infrastrutture e dei trasporti (2018). DM 17/01/2018 – Aggiornamento delle Norme Tecniche per le Costruzioni, Gazzetta Ufficiale, Serie Generale, 42, Supplemento Ordinario, 8, 20 febbraio 2018.

Nakamura, Y. (1989). A Method for Dynamic Characteristics Estimation of Subsurface using Microtremor on the Ground Surface, Quarterly Report of Railway Technical Research Institute-RTRI, 30, 1.

Nakamura, Y. (2000). Clear Identification of Fundamental Idea of Nakamura's Technique and Its Applications, The 12th World Conference on Earthquake Engineering, Auckland, New Zealand, 30 January-4 February 2000.

Nogoshi, M. and T. Igarashi (1971). On the Amplitude Characteristics of Microtremor, Part 2, in Japanese with English abstract, Jour. Seism. Soc. Japan, 24, 26-40.

Ohta, Y. (1963). On the Phase Velocity and Amplitude Distribution of Rayleigh Type Waves in Stratified Double Layer (in case of $\lambda \neq \mu$), in Japanese with English abstract, Zisin, 2, 16, 12-25.

Panzera, F., P. Bergamo, L. Danciu and F. Donat (2024). Investigating worldwide strong motion databases to derive a collection of free-field records to select design-compatible waveforms for Switzerland, Bull Earthquake Eng., 22, 4843-4872 doi:10.1007/s10518-024-01970-5.

Peterson, J. (1993). Observations and modeling of seismic background noise, U. S. Geol. Surv. Open File Report, 93-322, 1-94, doi:10.3133/ofr93322.

Pilz, M., F. Cotton and S. R. Kotha (2020). Data driven and machine learning identification of seismic reference stations in Europe, Geophys. J. Int., 222, 2, 861-873, doi:10.1093/gji/ggaa199.

SESAME (2004). Guidelines for the Implementation of the H/V Spectral Ratio Technique on Ambient Vibrations Measurements, Processing, and Interpretation, European Commission, Research General Directorate, 62, European Commission, Research General Directorate, sesame.geopsy.org.

Spudich, P., M. Hellweg and W. H. K. Lee (1996). Directional topographic site response at Tarzana observed in aftershocks of the 1994 Northridge, California, earthquake: Implications for mainshock motions, Bull. Seismol. Soc. Am., 86, 1B, S193-S208, doi:10.1785/BSSA08601BS193.

Van Houtte, C., O. J. Ktenidou, T. Larkin and A. Kaiser (2012). Reference stations for Christchurch, Bull. N. Z. Soc. Earth. Eng., 45, 4, 184-195, doi:10.5459/bnzsee.45.4.184-195.

Vantassel, J. (2020). Jpvantassel/hvsrpy: latest, Concept, Zenodo, doi:10.5281/zenodo.3666956.

Wessel, P., J. F. Luis, L. Uieda, R. Scharroo et al. (2019). The Generic Mapping Tools Version 6, Geochem. Geophys. Geosyst., 20, 11, 5556-5564, doi:10.1029/2019GC008515.

Appendix A.

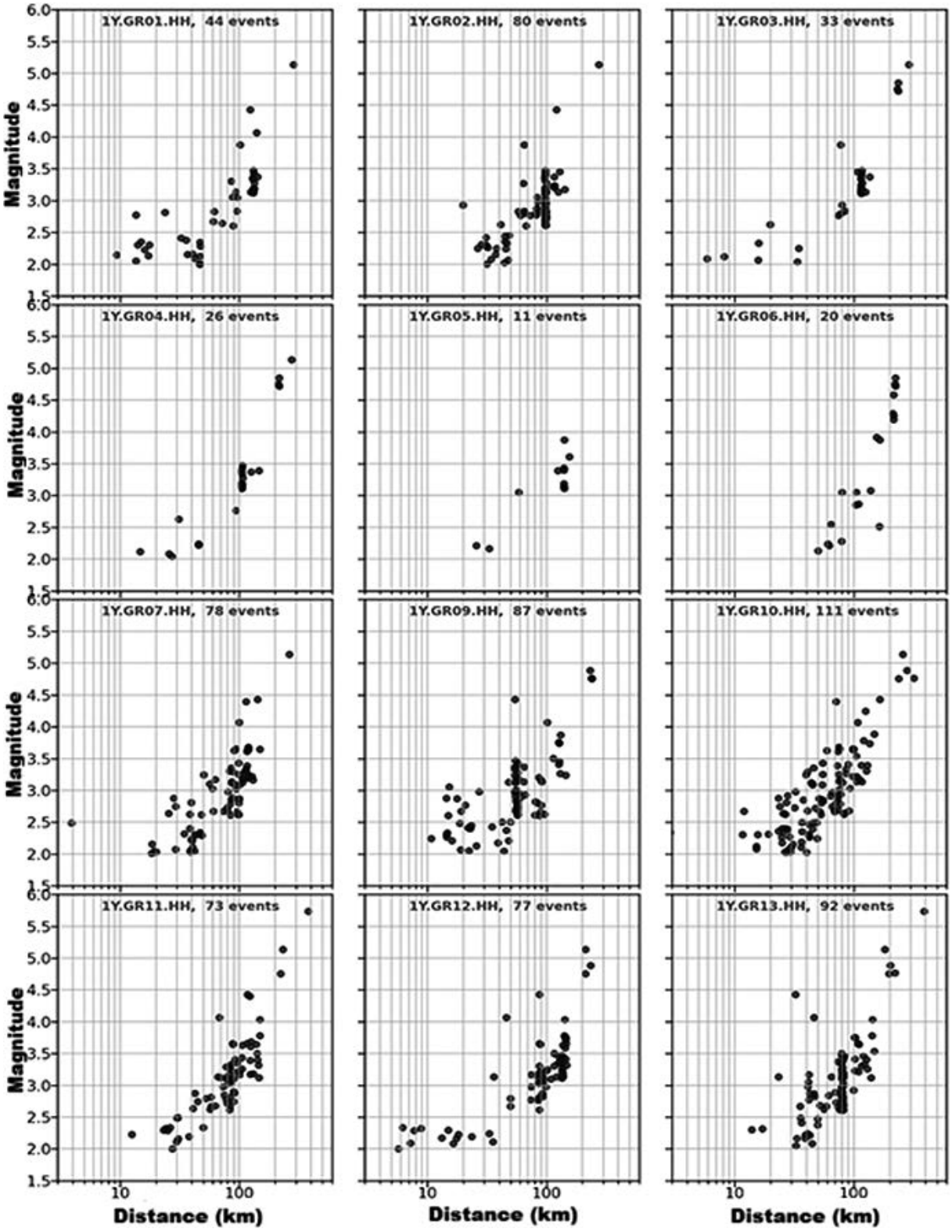
1Y.GR01.HH, 44 events
1Y.GR02.HH, 80 events
1Y.GR03.HH, 33 events
1Y.GR04.HH, 26 events
1Y.GR05.HH, 11 events
1Y.GR06.HH, 20 events
1Y.GR07.HH, 78 events
1Y.GR09.HH, 87 events
1Y.GR10.HH, 111 events
1Y.GR11.HH, 73 events
1Y.GR12.HH, 77 events
1Y.GR13.HH, 92 events
Magnitude
Distance (km)
6.0
5.5
5.0
4.5
4.0
3.5
3.0
2.5
2.0
1.5
10
100

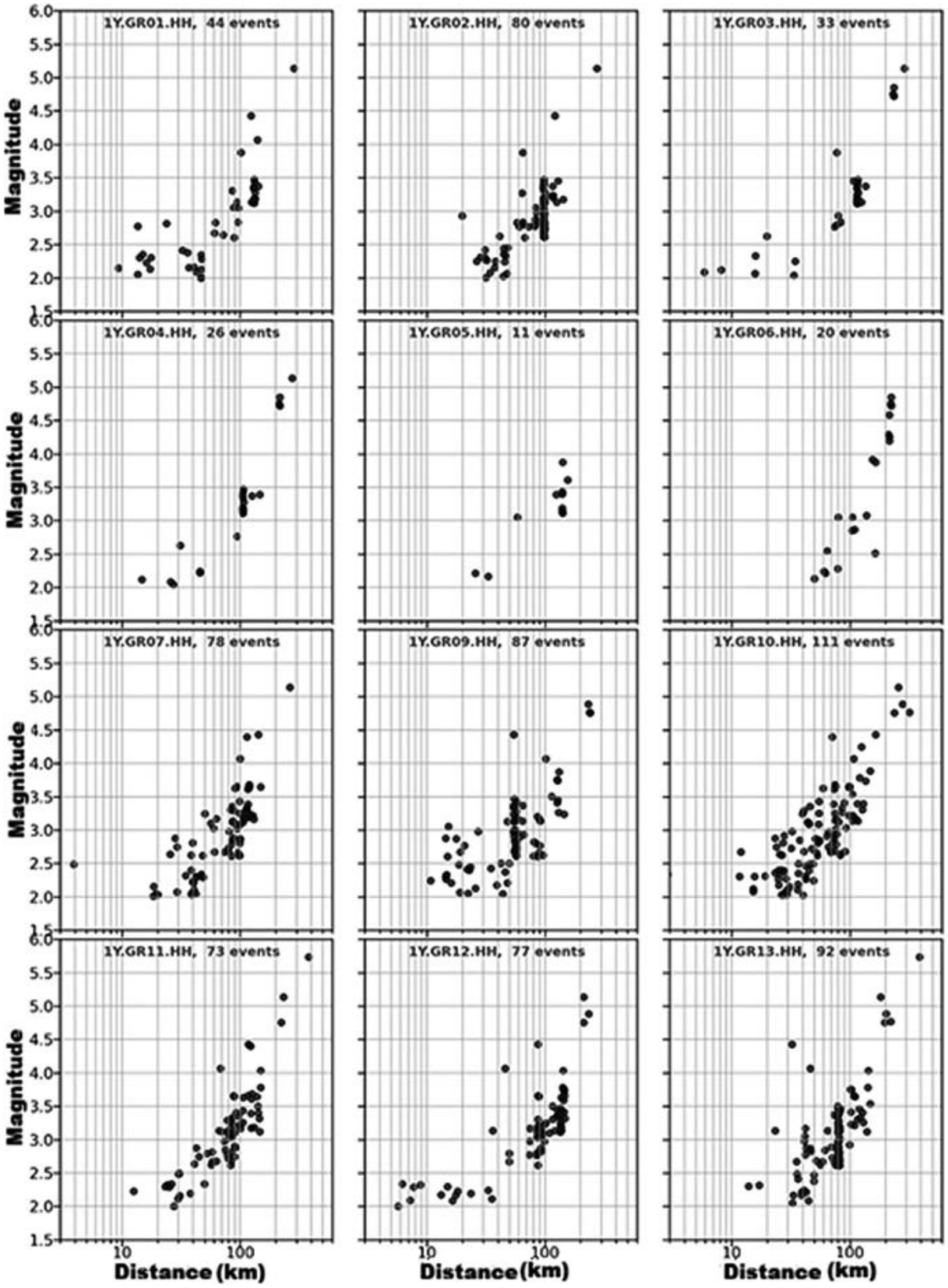
1Y.GR01.HH, 44 events
1Y.GR02.HH, 80 events
1Y.GR03.HH, 33 events
1Y.GR04.HH, 26 events
1Y.GR05.HH, 11 events
1Y.GR06.HH, 20 events
1Y.GR07.HH, 78 events
1Y.GR09.HH, 87 events
1Y.GR10.HH, 111 events
1Y.GR11.HH, 73 events
1Y.GR12.HH, 77 events
1Y.GR13.HH, 92 events
Magnitude
Distance (km)
6.0
5.5
5.0
4.5
4.0
3.5
3.0
2.5
2.0
1.5
10
100

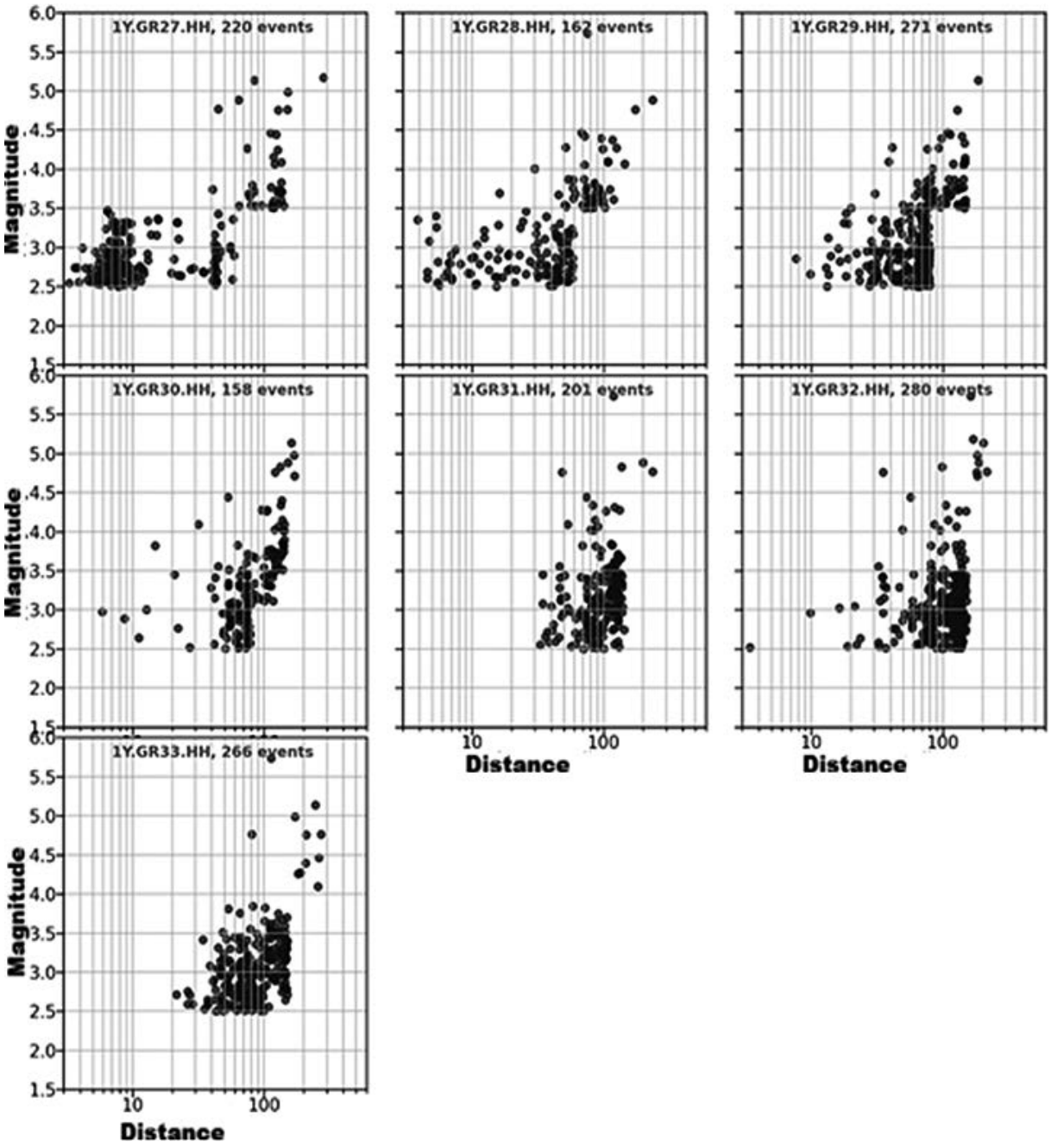

Figure A1. Distribution of magnitude (ML) and distance (epicentral) per station.

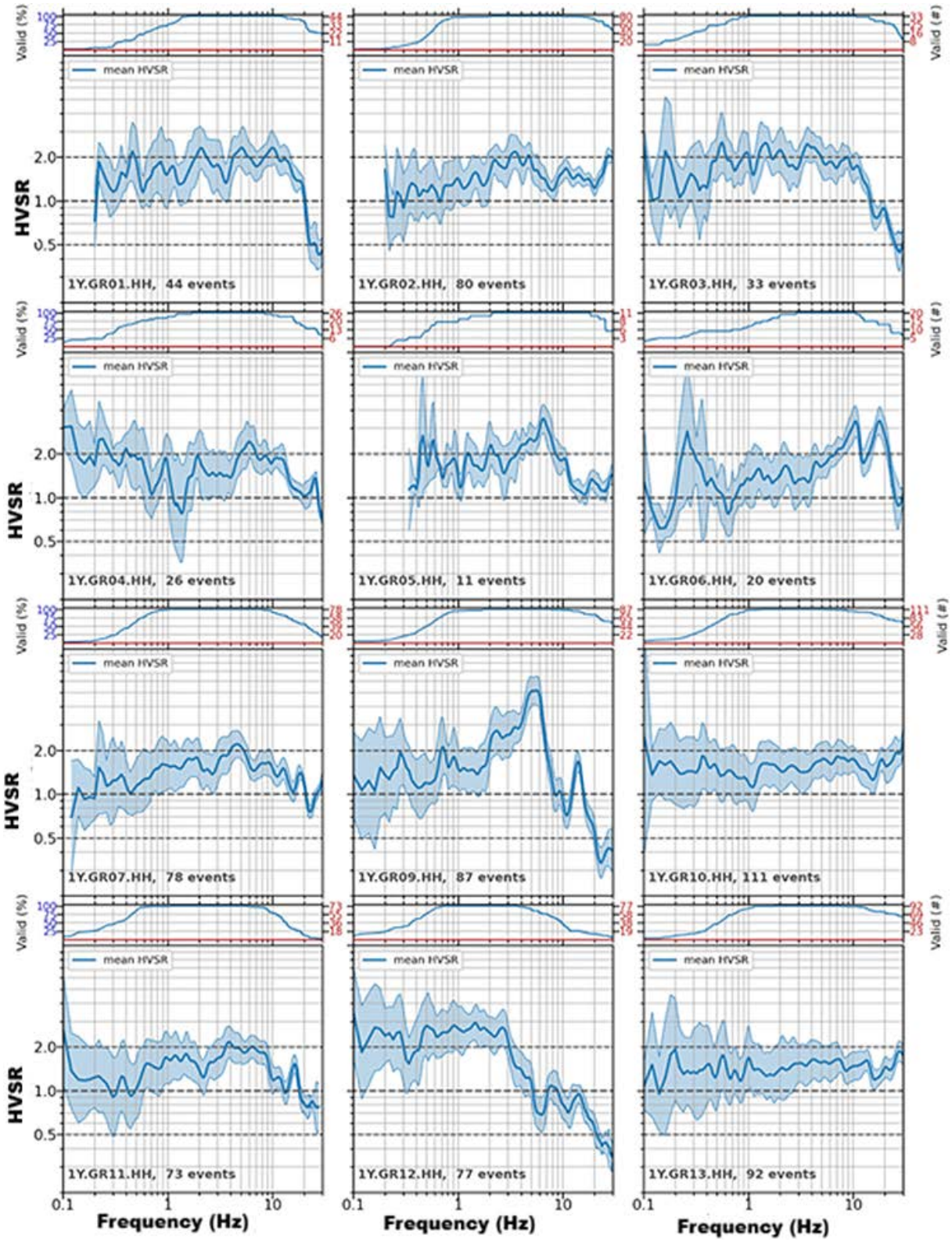
Valid (%)
Valid (#)
mean HVSR
HVSR
1Y.GR01.HH, 44 events
1Y.GR02.HH, 80 events
1Y.GR03.HH, 33 events
1Y.GR04.HH, 26 events
1Y.GR05.HH, 11 events
1Y.GR06.HH, 20 events
1Y.GR07.HH, 78 events
1Y.GR09.HH, 87 events
1Y.GR10.HH, 111 events
1Y.GR11.HH, 73 events
1Y.GR12.HH, 77 events
1Y.GR13.HH, 92 events
Frequency (Hz)

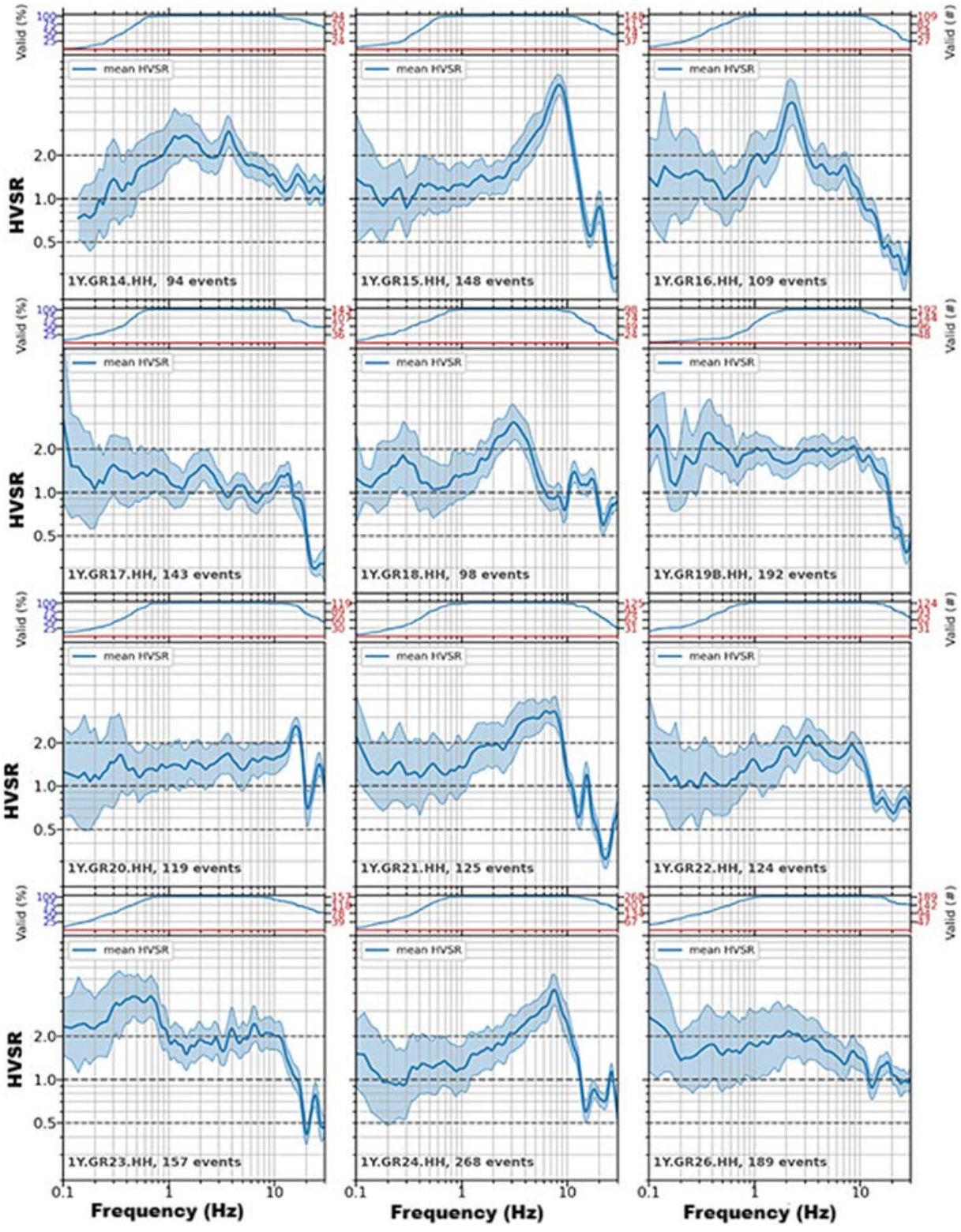
Valid (%)
Valid (#)
mean HVSR
HVSR
2.0
1.0
0.5
1Y.GR14.HH, 94 events
1Y.GR15.HH, 148 events
1Y.GR16.HH, 109 events
1Y.GR17.HH, 143 events
1Y.GR18.HH, 98 events
1Y.GR19B.HH, 192 events
1Y.GR20.HH, 119 events
1Y.GR21.HH, 125 events
1Y.GR22.HH, 124 events
1Y.GR23.HH, 157 events
1Y.GR24.HH, 268 events
1Y.GR26.HH, 189 events
0.1
1
10
Frequency (Hz)

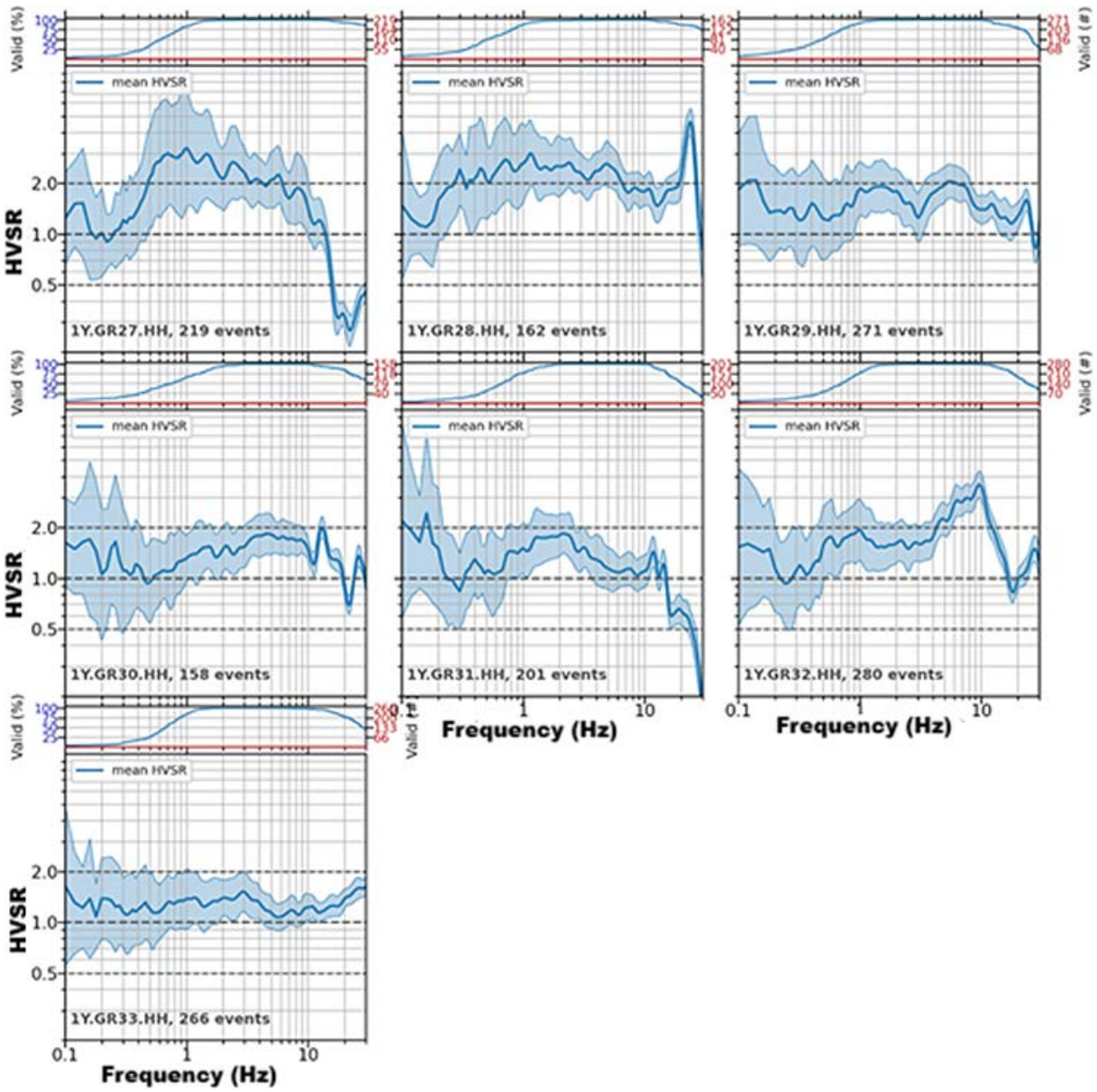

Figure A2. Mean orientation-invariant (SRSS) HVSR±1 standard deviation for all stations. Dashed horizontal lines indicate a factor of 2 from unity.

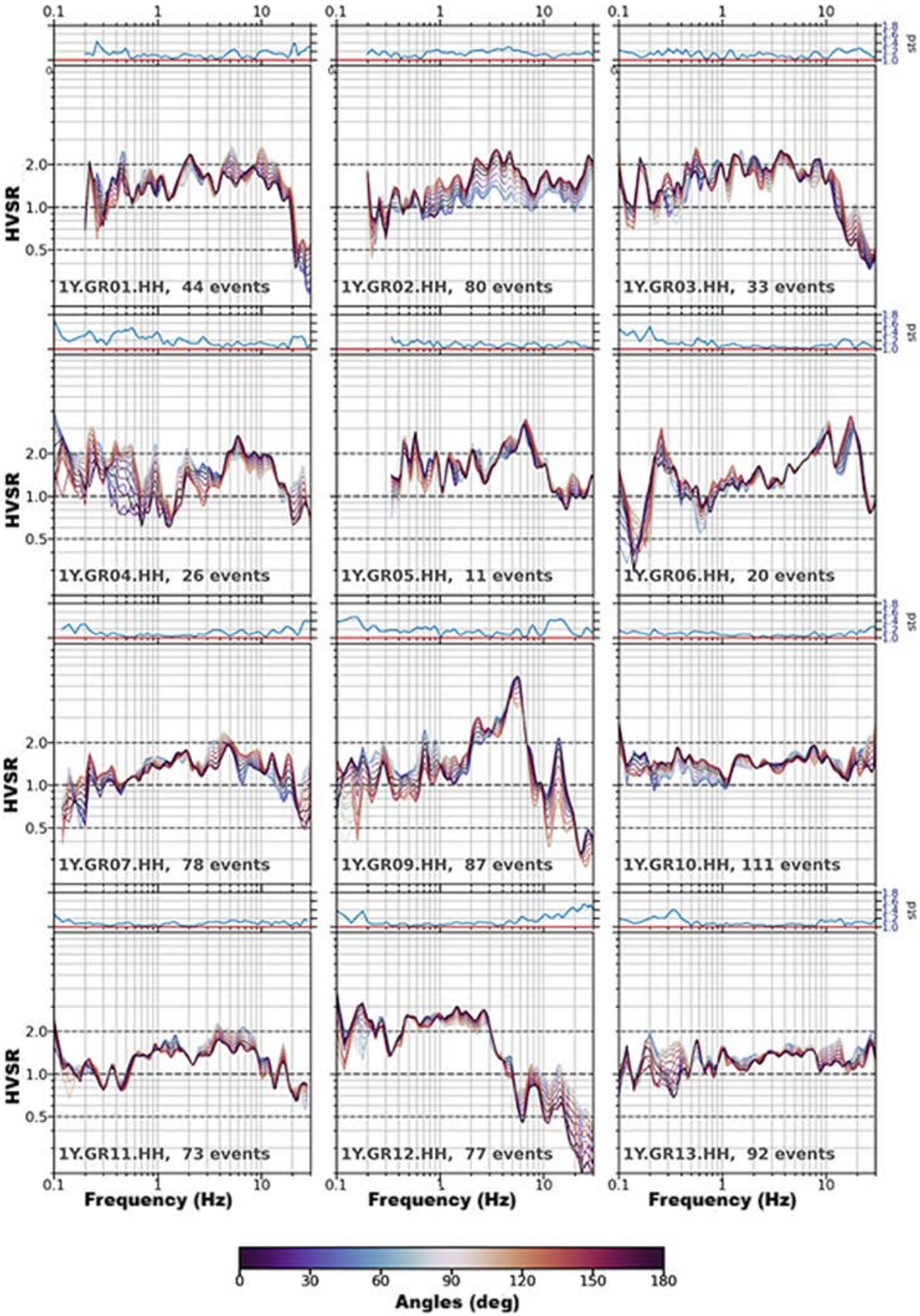
HVSR
std
1Y.GR01.HH, 44 events
1Y.GR02.HH, 80 events
1Y.GR03.HH, 33 events
1Y.GR04.HH, 26 events
1Y.GR05.HH, 11 events
1Y.GR06.HH, 20 events
1Y.GR07.HH, 78 events
1Y.GR09.HH, 87 events
1Y.GR10.HH, 111 events
1Y.GR11.HH, 73 events
1Y.GR12.HH, 77 events
1Y.GR13.HH, 92 events
Frequency (Hz)
Angles (deg)

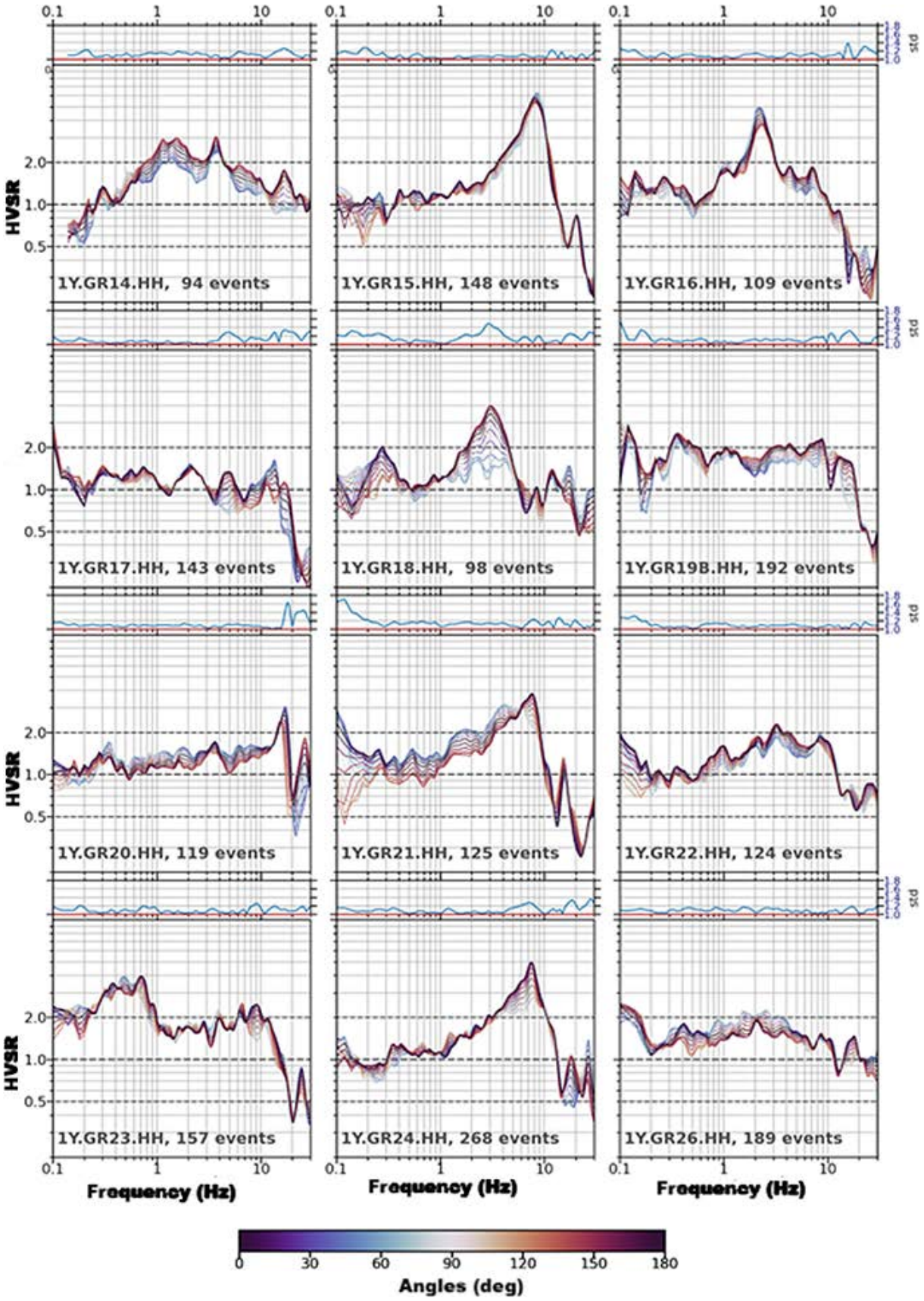
HVSR
std
1Y.GR14.HH, 94 events
1Y.GR15.HH, 148 events
1Y.GR16.HH, 109 events
1Y.GR17.HH, 143 events
1Y.GR18.HH, 98 events
1Y.GR19B.HH, 192 events
1Y.GR20.HH, 119 events
1Y.GR21.HH, 125 events
1Y.GR22.HH, 124 events
1Y.GR23.HH, 157 events
1Y.GR24.HH, 268 events
1Y.GR26.HH, 189 events
Frequency (Hz)
Angles (deg)

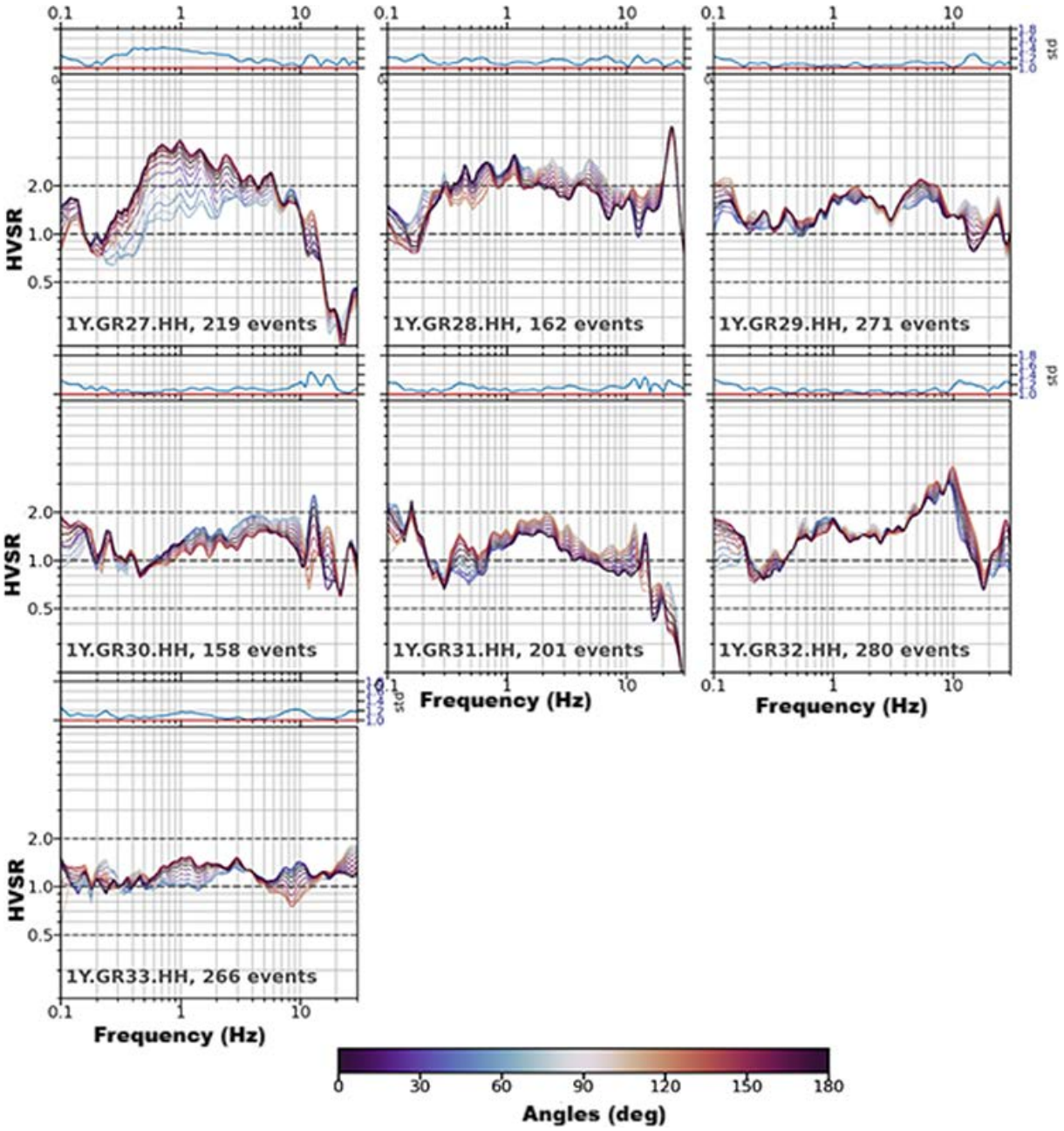

Figure A3. HVSR per component, as those are rotated by 10-degree intervals from North to East for all stations. Dashed horizontal lines indicate a factor of 2 from unity.

***CORRESPONDING AUTHOR: Antonia PAPAGEORGIOU**,
Institute of Geodynamics, National Observatory of Athens, Lofos Nymfon, Thiseio, Greece
e-mail: antoniapapageorgiou@gmail.com